Journal of the American Heart Association

ORIGINAL RESEARCH

Pericytes and Extracellular Vesicle Interactions in Neurovascular Adaptation to Chronic Arterial Hypertension

Lorena Morton, MD, PhD; Alejandra P. Garza, MD, MSc; Grazyna Debska-Vielhaber, PhD; Luis E. Villafuerte, MD, MSc; Solveig Henneicke, PhD; Philipp Arndt; Sven G. Meuth, MD, PhD; Stefanie Schreiber, MD, PhD; Ildiko R. Dunay, PhD

BACKGROUND: Chronic arterial hypertension restructures the vascular architecture of the brain, leading to a series of pathological responses that culminate in cerebral small-vessel disease. Pericytes respond dynamically to vascular challenges; however, how they manifest under the continuous strain of hypertension has not been elucidated.

METHODS AND RESULTS: In this study, we characterized pericyte behavior alongside hypertensive states in the spontaneously hypertensive stroke-prone rat model, focusing on their phenotypic and metabolic transformation. Flow cytometry was used to characterize pericytes by their expression of platelet-derived growth factor receptor β, neuroglial antigen 2, cluster of differentiation 13–alanyl aminopeptidase, and antigen Kiel 67. Microvessels were isolated for gene expression profiling and in vitro pericyte expansion. Immunofluorescence validated the cell culture model. Plasma-derived extracellular vesicles from hypertensive rodents were applied as a treatment to assess their effects on pericyte function and detailed metabolic assessments on enriched pericytes measured oxidative phosphorylation and glycolysis. Our results reveal a shift in platelet-derived growth factor receptor β^+ pericytes toward increased neuroglial antigen 2 and cluster of differentiation 13–alanyl aminopeptidase coexpression, indicative of their critical role in vascular stabilization and inflammatory responses within the hypertensive milieu. Significant alterations were found within key pathways including angiogenesis, blood–brain barrier integrity, hypoxia, and inflammation. Circulating extracellular vesicles from hypertensive rodents distinctly influenced pericyte mitochondrial function, evidencing their dual role as carriers of disease pathology and potential therapeutic agents. Furthermore, a shift toward glycolytic metabolism in hypertensive pericytes was confirmed, coupled with ATP production dysregulation.

CONCLUSIONS: Our findings demonstrate that cerebral pericytes undergo phenotypic and metabolic reprogramming in response to hypertension, with hypertensive-derived plasma-derived extracellular vesicles impairing their mitochondrial function. Importantly, plasma-derived extracellular vesicles from normotensive controls restore this function, suggesting their potential as both therapeutic agents and precision biomarkers for hypertensive vascular complications. Further investigation into plasma-derived extracellular vesicle cargo is essential to further explore their therapeutic potential in vascular health.

Key Words: blood–brain barrier ■ extracellular vesicles ■ hypertension ■ mitochondrial membrane potential ■ pericytes ■ spontaneously hypertensive stroke-prone rat (SHRSP) ■ vascular remodeling

Cerebral microvasculature is essential for brain health, playing a pivotal role in maintaining vascular stability and homeostasis.[1–6] Pericytes, central to the integrity of the blood–brain barrier (BBB),[7,8] regulate blood flow[9,10] and angiogenesis[11] and orchestrate vascular immune homeostasis of the neurovascular

Correspondence to: Ildiko Rita Dunay, PhD, Medical Faculty, Institute of Inflammation and Neurodegeneration, Otto-von-Guericke University Magdeburg, Leipziger Str. 44, 39120 Magdeburg, Germany. Email: ildiko.dunay@med.ovgu.de

Supplemental Material is available at https://www.ahajournals.org/doi/suppl/10.1161/JAHA.124.038457

Preprint posted on BioRxiv May 15, 2024. doi: https://doi.org/10.1101/2024.05.13.594041.

This manuscript was sent to Neel S. Singhal, MD, PhD, Associate Editor, for review by expert referees, editorial decision, and final disposition.

For Sources of Funding and Disclosures, see page 20.

JAHA is available at: www.ahajournals.org/journal/jaha

RESEARCH PERSPECTIVE

What Is New?

- Our findings reveal significant pericyte phenotypic and metabolic shifts under hypertensive conditions, specifically a glycolytic shift and an increased neuroglial antigen 2 and cluster of differentiation 13–alanyl aminopeptidase expression.
- We demonstrated the novel role of extracellular vesicles in transmitting hypertensive signals that impair mitochondrial function in normotensive pericytes.

What Question Should Be Addressed Next?

- Future research should focus on identifying the specific molecular cargo of extracellular vesicles to understand how their contents from hypertensive versus normotensive sources affect pericyte function and vascular health.
- To explore the therapeutic potential of extracellular vesicles derived from healthy controls to mitigate vascular and mitochondrial dysfunction in hypertensive conditions, which could open treatment strategies for vascular health management.

Nonstandard Abbreviations and Acronyms

BBB	blood–brain barrier
cSVD	cerebral small-vessel disease
CD13	cluster of differentiation 13–alanyl aminopeptidase
EVs	extracellular vesicles
NG2	neuroglial antigen 2
pdEVs	plasma-derived extracellular vesicles
PDGFRβ	platelet-derived growth factor receptor β
SHRSP	spontaneously hypertensive stroke-prone rat

unit,[12–15] thereby collectively contributing to immunosurveillance and overall cerebrovascular health. Their dysfunction has been implicated in a range of cerebrovascular diseases, from stroke to dementia, indicating their importance across various pathologies.[16–21] In conditions such as chronic arterial hypertension,[22] pericyte dysfunction may be linked to BBB disruption by endothelial cell malfunction, cerebrovascular remodeling, and the onset of cerebral small-vessel disease (cSVD).[23,24] cSVD is characterized by white matter lesions, vascular-associated activated microglia states, and microvascular abnormalities, exacerbated by chronic inflammation associated with aging and chronic arterial hypertension.[25–29] Among its subtypes, arteriolosclerosis, marked by thickening and stiffening of vessel walls, is prevalent in older adults and in those with vascular risk factors, significantly altering cerebral microcirculation and heightening ischemic vulnerability.[30]

Extracellular vesicles (EVs) have gained attention recently for their role in cellular communication, influencing the behavior of cells through the transfer of bioactive molecules.[31,32] These vesicles, which are shed by all cell types into the circulation, facilitate a unique cellular interaction by carrying a cargo of proteins, lipids, and nucleic acids, capable of modulating recipient cell function and contributing to disease processes.[33]

Pericytes respond dynamically to vascular challenges; however, the specific responses under the continuous strain of hypertension has not been elucidated. Here, using the spontaneously hypertensive stroke-prone rat (SHRSP),[34,35] which closely mimics hypertensive cSVD in humans,[24,36–38] we examine how pericytes adapt to prolonged arterial hypertension. We demonstrate how pericytes respond to hypertensive stress by altering their phenotype and metabolic pathways early in disease onset. We revealed that in the face of systemic hypertension, pericytes increase their dependence on glycolytic pathways, a metabolic shift that might initially serve adaptive purposes but becomes maladaptive. This shift is accompanied by significant changes in the expression of platelet-derived growth factor receptor ß (PDGFRß), neuroglial antigen 2 (NG2), and cluster of differentiation 13–alanyl aminopeptidase (CD13), canonical pericyte markers.[39,40] We also provide novel evidence on the metabolic reprogramming of pericytes in chronic arterial hypertension and the involvement of EVs in mediating vascular pathology across the neurovascular unit.

METHODS

The data that support the findings of this study are available from the corresponding author upon reasonable request.

Animals

All experiments were conducted in compliance with the Animal Research: Reporting of In Vivo Experiments guidelines,[41] adhered to the German Animal Welfare Ordinance, and were approved by the Animal Care Committee of Saxony-Anhalt (license identification numbers 42502-2-1277 for Uni MD) following institutional guidelines. A total of 116 male rats were used across various experimental phases, as detailed

in Table S1. For the initial hypertension phase, we refer to 6- to 8-week-old Wistar rats (control) and SHRSPs. The early chronic hypertension phase includes 25-week-old rats, and the late chronic hypertension phase comprises 34- to 36-week-old rats. All animals were sourced from Charles River Laboratories (Wilmington, MA, for SHRSP; Research Models and Services, Germany GmbH, Sulzfeld, Germany for Wistar rats). Wistar rats served as controls, while SHRSP rats model hypertension at specified ages, which reflect the progression from initial to late chronic hypertension.[35,36] All animals were housed with a natural light–night cycle, had access to water and food ad libitum, and were monitored daily to assess neurological functions. SHRSPs develop a vascular risk profile characterized by arterial hypertension from 6 weeks of age and develop classical cSVD pathology.[37,38,42]

Vascular Cell Isolation for Flow Cytometry

To characterize pericytes and endothelial cells, vascular cells were isolated from 6-, 25-, and 34-week-old control and hypertensive rats using a modified version of the study by Crouch et al, adapted for rat brains.[43] Following anesthesia with pentobarbital and hemisphere preparation, cerebral cortices were enzymatically dissociated at 37 °C for 30 minutes with collagenase/dispase (Sigma-Aldrich; Catalog No. 11097113001) at optimized concentrations (3.33 mg/mL) for 0.9 grams of tissue following suggested concentrations, mechanically triturated with DNase (Worthington; Catalog No. 2139), and purified using a 22% Percoll gradient (Sigma-Aldrich; Catalog No. GE17-0891-01). Isolated cells were washed, counted, centrifuged, resuspended, and stained. Unstained cells, fluorescence minus one, and single-staining controls with compensation beads were used as controls. Prior to fluorochrome-conjugated antibody labeling, cells were incubated with purified mouse anti-rat CD32 FcγII (clone D34-485, Rat BD Fc Block) for unspecific binding. Cell viability was assessed using a dead dye (Zombie NIR; Biolegend), and cells were stained with a panel of fluorophore-conjugated antibodies, including anti-CD45 (clone: OX-1), anti-CD31 (clone: TLD-3A12), anti-PDGFRß (clone: rabbit polyclonal), anti-NG2 (clone: D120.43), and anti-CD13 (clone: WM15), followed by fixation, permeabilization, and anti–antigen Kiel 67 (Ki-67; clone: SolA15) staining. Data were acquired and analyzed using AttuneNxT (Thermo Fisher Scientific) and Flowjo Analysis Software version 10.5.3 (BD). Uniform manifold approximation and projection analysis was performed on exported live, single, CD45-negative, CD31, and PDGFRß-positive cells downsampled to 7500 cells per group and time point. Concatenated data were projected to uniform manifold approximation and projection using vascular compensated markers and 25 nearest neighbors with a minimum distance of 0.8 as running parameters.

Tissue Dissociation and Microvessel Isolation

Brains from control and hypertensive rats aged 8, 25, and 34 weeks were harvested following transcardial perfusion with PBS-EDTA for microvessel isolation using already established optimized protocols.[29,44,45] Briefly, cortices were mechanically dissociated by mincing the tissue into fine fragments and enzymatically digested with collagenase type II (1 mg/mL) and DNase I (15 μg/mL) in DMEM/F12 containing penicillin (100 units/mL), streptomycin (100 μg/mL), and glutamine (2 mM). Myelin and neurons were removed via centrifugation in 20% BSA-DMEM/F12 at 1000 *g* for 20 minutes, repeating the process 3 times. Microvessels were collected from pellets into new sterile tubes and further digested with collagenase-dispase (1 mg/mL) and DNase I (6.7 μg/mL) in DMEM for 60 minutes at 37 °C. Microvessels were layered on top of a 33% Percoll (Sigma-Aldrich; Catalog No. GE17-0891-01) density gradient and centrifuged for 10 minutes at 1000 *g* at 4 °C. Microvessels were washed twice, filtered through a 40-μm cell strainer, reversed, washed into a new sterile tube, and centrifuged at 400 *g* for 10 minutes at 4 °C. Microvessels were assessed microscopically before being stored in RNAlater (AM7020; Thermo Fisher Scientific) for further processing, or seeded for in vitro culture assays for pericyte in vitro expansion.

RNA Isolation and RT2 Profiler Polymerase Chain Reaction Array

Collected microvessels were pelleted at 20000 *g* for 10 minutes and resuspended in 350 μL of RLT Plus Buffer from the RNeasy Micro Kit (QIAGEN). RNA was isolated using the RNeasy Plus Micro Kit, following the manufacturer's instructions, as previously described.[29] RNA quality was determined using a NanoDrop 2000 (Thermo Fisher Scientific) spectrophotometer and used in combination with Power SYBR Green RNA-to-CT 1-Step Kit (Thermo Fisher Scientific; Catalog No. 4389986) on a custom RT^2 profiler polymerase chain reaction array (QIAGEN) using a LightCycler 96 (Roche). Cycle threshold values were exported to an Excel file to create a table. This table was then uploaded to the data analysis web portal at http://www.qiagen.com/geneglobe. Samples were assigned to control and test groups. Cycle threshold values were normalized on the basis of the selection of reference genes. The data analysis web portal calculated fold change and gene regulation using the $2-\Delta\Delta Ct$ method.[46] The *Hprt* gene was used to normalize the results. Data were further normalized to the respective mean level in age-matched early control. The full

list of genes included in the custom polymerase chain reaction array is provided in Table S2. Downstream gene ontology analyses, data presentation, and statistical analyses of exported gene regulation tables were performed using STRING database version 12.0 and Prism 10 (GraphPad Software).

Pericyte In Vitro Subculture

Rat cerebral pericytes were cultured from isolated brain microvessels containing a mix of pericytes and endothelial cells. Initial microvessel seeding was established in DMEM/F12 supplemented with 15% platelet-derived serum, 1 ng/mL basic fibroblast growth factor, and 100 μg/mL heparin for the first 2 days. The medium was then switched to DMEM supplemented with 10% FBS, 1% nonessential amino acids, and 1% penicillin/streptomycin to support pericyte survival and proliferation. To enrich pericyte populations and eliminate endothelial cells, cultures were treated in the absence of puromycin, allowing pericyte expansion. Subsequent cell expansions were done using Accutase Cell Solution (Biolegend) for gentle detachment, ensuring optimal cell viability. For cryopreservation, cultures were frozen in CryoStor CS10 (Stemcell Technologies) and stored in liquid nitrogen.

Immunofluorescence Staining

Pericytes were expanded in vitro from seeded 8-week-old rat microvessels. At passages 11 to 13, pericytes at 90% to 95% confluence from T-75 cell culture flasks (Greiner CELLSTAR) were seeded at a density of 20 000 cells/well in 12-well plates containing 20-mm coverslips. Coverslips were sterilized and coated with rat tail collagen 24 hours before pericyte expansion. Cells were fixed with 4% PFA and washed 48 hours after seeding. Thereafter, cells were blocked with 3% horse serum for 2 hours. Primary antibodies were incubated overnight at room temperature in the same solution. After PBS washes, cells were incubated with secondary antibodies diluted 1:1000 in 0.1% Triton X-100. Mounting was performed with ProLong mounting medium containing DAPI (Thermo Fisher Scientific; Catalog No. P36935), and coverslips were dried in darkness before microscopy analysis. Imaging was performed to visualize and confirm pericyte identity and purity using a TCS SP8 X Laser Confocal Microscope (Leica Microsystems) software (LAS-AF 1.8.1.13759). A full list of antibodies and their specificities can be found in Table S3.

Immunofluorescence Image Processing and Analysis

Immunofluorescence images were processed using ImageJ (Rasband, [https://imagej.nih.gov/ij/, 1997–2018]) and viewed as hyperstacks in default color mode. The scale was changed from grayscale to specific colors for each channel. Channels were split, with contrast and brightness adjusted uniformly across samples to maintain consistent parameters. Individual adjusted and composite images created were saved as TIFF files. For z-stack images, after color adjustment and maximum intensity projection, images were processed similarly by splitting and merging channels, as described above, with the final composite image converted to RGB and saved as TIFF. The mean fluorescence intensity of PDGFRβ, NG2, and CD13 from individual cells was exported from processed images, as described previously.[47] Quantitative data were used to plot the mean fluorescence intensity for each marker, allowing for the analysis of expression patterns in control versus hypertensive pericytes.

Flow Cytometric Analysis of In Vitro Pericytes

At passages 11 to 13, pericytes at 90% to 95% confluence from T-75 cell culture flasks were dissociated with Accutase Cell Solution (BioLegend) and prepared for flow cytometry to analyze subtype distribution in vitro, comparing control versus hypertensive-derived cells. Cells were stained with antibodies against PDGFRβ, NG2, and CD13 and analyzed using an Attune NxT Flow Cytometer. Fluorescence minus one controls and unstained samples were used to set gates. Postacquisition data analysis was performed using FlowJo software version 10.5.3. Data were biexponentially transformed for scaling and t-distributed stochastic neighbor embedding was employed on compensated PDGFRβ-positive cells at a perplexity of 10 and 1500 iterations to examine the differential expression of CD13 and NG2 in control versus hypertensive pericytes.

Plasma-Derived Extracellular Vesicles

Peripheral blood was collected from the portal vein of anesthetized animals using a 21G butterfly needle, immediately mixed with acid citrate dextrose, and subjected to 2 inversions for agent incorporation. Samples were processed within 1 hour, as previously described.[48] Briefly, plasma separation was initially achieved by centrifugation at 1500*g* for 10 minutes, which was then transferred to sterile 1.5-mL Eppendorf tubes. To isolate EVs, the plasma underwent 2 centrifugation cycles at 1500*g* for 10 minutes maintaining supernatant, followed by 2 rounds of ultracentrifugation at 14 000*g* for 70 minutes, discarding supernatants and resuspending pellets in 0.22-μm filtered PBS (–/–). The final EV pellet was resuspended in 200 μL of filtered PBS –/– and stored at –80 °C. For EV characterization, 10 μL of isolated EVs was then mixed with 90 μL of filtered PBS –/–, and samples were labeled with CD9, CD63, and CD81 (APC-conjugated,

Clones HI9A, H5C6 and 5A6, respectively; Biolegend). Samples were analyzed using an Attune NxT Flow Cytometer equipped with a small particle side scatter filter. Size gating (300–1000 nm) was established using silica beads (Creative Diagnostics). Acquisition of samples was performed at a speed of 25 μL per minute, with side scatter threshold set to 0.18×10^3 and forward scatter threshold set to 0.15×10.[3] A stop option was activated upon reaching 150 000 events within the size gate. Each sample measurement was followed by a 10% bleach and 0.22-μm filtered distilled water rinse. Data analysis was conducted using FlowJo 10.9.0 and GraphPad Prism 10 for subsequent downstream analyses.

JC-10 Mitochondrial Membrane Potential Assay

At passages 11 to 13, enriched pericytes at 90% to 95% confluence from T-75 cell flasks derived from control and hypertensive rodents, respectively, were expanded and seeded in 96-well plates at a density of 10 000 cells/well for 24 hours prior. Cells were subjected to a JC-10 mitochondrial membrane potential assay (BioLegend; Catalog No. 421902) to assess metabolic responses to plasma and plasma-derived extracellular vesicles (pdEVs). Before stimulation cells were incubated in pericyte ultracentrifuged (18 hours × 110 000 *g*) basal medium containing 1% fetal calf serum. Treatments included 10% v/v normotensive or hypertensive plasma, or normotensive or hypertensive pdEVs standardized to a protein concentration of 13.5 μg. All stimulations were induced for 6 hours. JC-10 dye was added following the manufacturer's instructions, and changes in mitochondrial membrane potential were measured by calculating the ratio of red/green fluorescence ratio indicative of mitochondrial health using the AttuneNxT and Flowjo Analysis Software version 10.5.3.

Extracellular Flux Analysis

Metabolic profiles of hypertensive and control rat pericytes were determined using a Seahorse XFp Extracellular Flux Analyzer (Agilent Technologies). Initial hypertension experiments represent aggregate data derived from 8 biological samples measured in triplicates at passages 5, 7, and 9 derived from 6-week-old rodents; and chronic hypertension experiments represent aggregate data derived from 10 biological samples measured in triplicates at passages 9, 11, and 13 derived from 25-week-old rodents. Mitochondrial respiration, glycolysis rate, and real-time ATP production rate were measured using suitable kits (Cell Mito Stress Test, Glycolysis Stress Test, Real-Time ATP Rate Assay) according to the manufacturer's instructions and as already shown.[49] Briefly, after cell harvesting, pericytes were resuspended in culture medium and seeded at 1.5×10^4 cells/well in Seahorse cell culture microplates and incubated overnight in a CO_2 incubator. After replacing the growth medium with prewarmed assay XF DMEM medium pH 7.4 supplemented with 1 mM pyruvate, 2 mM glutamine, and 10 mM glucose for Mito Stress Test and ATP production rate and only with 2 mM glutamine for Glycolysis Stress Test, the cells were preincubated at 37 °C for 45 minutes in a non-CO_2 incubator. The cartridges were loaded with assay medium and with standard inhibitors/substrates: 5 μM oligomycin, 2.25 μM FCCP, and 1 μM rotenone/ antimycin A mixture for Mito Stress Test and with 10 mM glucose, 5 μM oligomycin, and 50 mM 2-deoxy-glucose for Glycolysis Stress Test or with 5 μM oligomycin and 1 μm rotenone/anitmycin A mix for ATP production rate measurement. For experiments with metabolic inhibitors, the first port of cartridge was loaded with a cocktail of mitochondrial inhibitors (2 μM UK5099, 3 μM BPTES, 4 μM Etomoxir or glycolysis inhibitor [50 mM 2-deoxyglucose]) and the last 3 ports with standard inhibitors. After the cartridges were calibrated, measurements were initiated. For ATP production rate measurements, the assay medium in cell microplates was again changed to a fresh one. The Seahorse assays were analyzed using XF Wave 2.6.1 software, according to manufacturer's instructions. After the measurements, cells were collected and lysed using RIPA buffer and diluted with PBS. Total protein concentrations were measured on an absorbance microplate reader Sunrise (TECAN) using BCA Protein Assay (Sigma-Aldrich). For all calculations, the oxygen consumption rate and extracellular acidification rate were normalized to the total amount of protein in each well and expressed per microgram of protein. Cell Mito Stress Test was used to investigate most important mitochondrial properties: proton leak, ATP-linked respiration, maximal respiration, and spare respiratory capacity. The Glycolysis Stress Test was used to study glycolytic function of pericytes, and ATP test to explore real-time ATP production rate in control and hypertensive pericytes.

Statistical Analysis

Data analysis was performed using GraphPad Prism 10 software. All data are shown as mean ± SEM, and exact numbers for each data set are detailed in figure legends. Data were assessed for normality. Parametric unpaired *t* tests were used to compare normally distributed data between 2 groups. For comparison between multiple groups, a 1-way ANOVA was used followed by Holm–Sidak to correct for multiple comparisons. For comparison between multiple groups and conditions, the data were analyzed using 2-way ANOVA followed by Holm–Sidak post hoc correction. *P* values ≤0.05 were considered to indicate statistical significance. During

experimental procedures, the principal investigator was aware of the group allocations between strains to coordinate the sequence of experiments. Blinding was implemented during specific assessments such as immunofluorescence stainings and the Seahorse metabolic analyses. Data analyses were initially conducted by blinded personnel, with group identities disclosed after analysis for final interpretation.

RESULTS

Stage-Specific Brain Vascular Cell Adaptation to Hypertensive Stress

In our cross-sectional study, we examined the effects of hypertension across 3 defined stages: initial hypertension, early chronic hypertension, and late chronic hypertension stages in the SHRSP model, on brain microvascular cells (Figure 1A, Figure S1A). We identified brain vascular cells, particularly focusing on differentiating endothelial cells (CD31$^+$) from pericytes (PDGFRß$^+$; Figure 1B; Figure S2A and S2B). Our initial identification of pericytes was based on the positive selection of PDGFRß, a marker that is expressed in all pericyte subtypes,[40] and subsequently subdivided pericytes on the basis of their expression of NG2 and CD13.[40] Our results showed that at the onset of hypertension, the frequency of CD31$^+$ endothelial cells and the vascular pericyte compartment remained consistent between groups (Figure 1C through 1E).

During early chronic hypertension (Figure 1F and 1G), the vascular system adapts to persistent midlife hypertensive conditions, resulting in enhanced expression of NG2 and double the amount of CD13 pericytes compared with controls (11% versus 23%, P=0.0335). A significant decrease was observed in frequency of PDGFRß$^+$ cells in hypertension (13% versus 8%, P=0.0399; Figure 1H), while the frequency of CD31$^+$ endothelial cells remained stable between groups. This result showed a specific susceptibility of pericytes to early chronic hypertensive stress (Figure 1H).

In the late chronic hypertension phase, NG2 expression dominated the pericyte population (Figure 1I and 1J). Quantitative analysis revealed that in controls, only a small fraction of PDGFRß$^+$ cells coexpressed CD13 (3%), while a substantial majority coexpressed NG2 (77%). In contrast with early chronic hypertension, CD13 co-expression decreased to 7%, NG2 coexpression remained the same, and PDGFRß$^+$ expression increased, marking a nuanced yet significant shift in pericyte subtypes (Figure 1J). Furthermore, we observed a significant increase in the frequency of CD31$^+$ endothelial cells in late chronic hypertension (20% versus 11% in controls, P<0.0001) and a modest rise in PDGFRß$^+$ hypertensive pericytes (12% versus 10% in controls, P=0.032; Figure 1K). Detailed statistical analysis of these changes across all hypertension phases can be found in Figure S1B, which highlight the overall reduction in brain vascular cell populations over the progression of hypertension.

Differential Proliferative Capacity of Brain Endothelial Cells and Pericytes in Hypertensive States

We conducted further analyses to investigate the proliferative responses of endothelial cells and pericytes across hypertension phases using Ki-67, a nuclear protein marker of cell proliferation, to indicate the fraction of cells undergoing division. In the initial hypertension (Figure 2A through 2D), while the absolute numbers of endothelial cells remained stable, there was a significant increase in Ki-67 expression in the hypertensive group (Figure 2A and 2B). Conversely, there were no discernible differences in the absolute numbers of PDGFRß$^+$ pericytes or their Ki-67 expression between control and hypertension displaying an early resilience in response to hypertensive stress (Figure 2C and 2D). In early chronic hypertension (Figure 2E through 2H), endothelial cells maintained stable numbers without the same proliferative increase observed in pericytes. During this phase, there was a significant reduction in the absolute number of pericytes in hypertension alongside an increase in Ki-67 expression, depicting pericytes under stress, both decreasing in number and increasing in proliferative activity (Figure 2G and 2H), pointing to a unique interplay between the cellular responses of each vascular component. In the late stage of chronic hypertension (Figure 2I and 2L), while endothelial cells displayed a significant increase in both numbers and Ki-67 expression in hypertension, our results showed a significant increase in the number of pericytes and a decrease in Ki-67 expression.

Tracing the Development of Vascular Markers in Hypertension Progression

Building on our comprehension of hypertension-associated vascular remodeling, we aimed to delineate the dynamic vascular profile throughout the progression of hypertension. Using uniform manifold approximation and projection analysis, we projected CD31$^+$ and PDGFRß$^+$ cells to discern between shifts in vascular cell properties (Figure 3A). We set to characterize different aspects of vascular cell behavior that underlie the significant changes observed in cellular marker expression and population dynamics across different stages of hypertension. We investigated the vascular identity of hypertension (Figure 3B), revealing a multifaceted landscape where CD31, PDGFRß, NG2, and CD13 expressions converge. This analysis revealed an evolving expression pattern of endothelial and pericyte markers, pinpointing the location of PDGFRß clusters

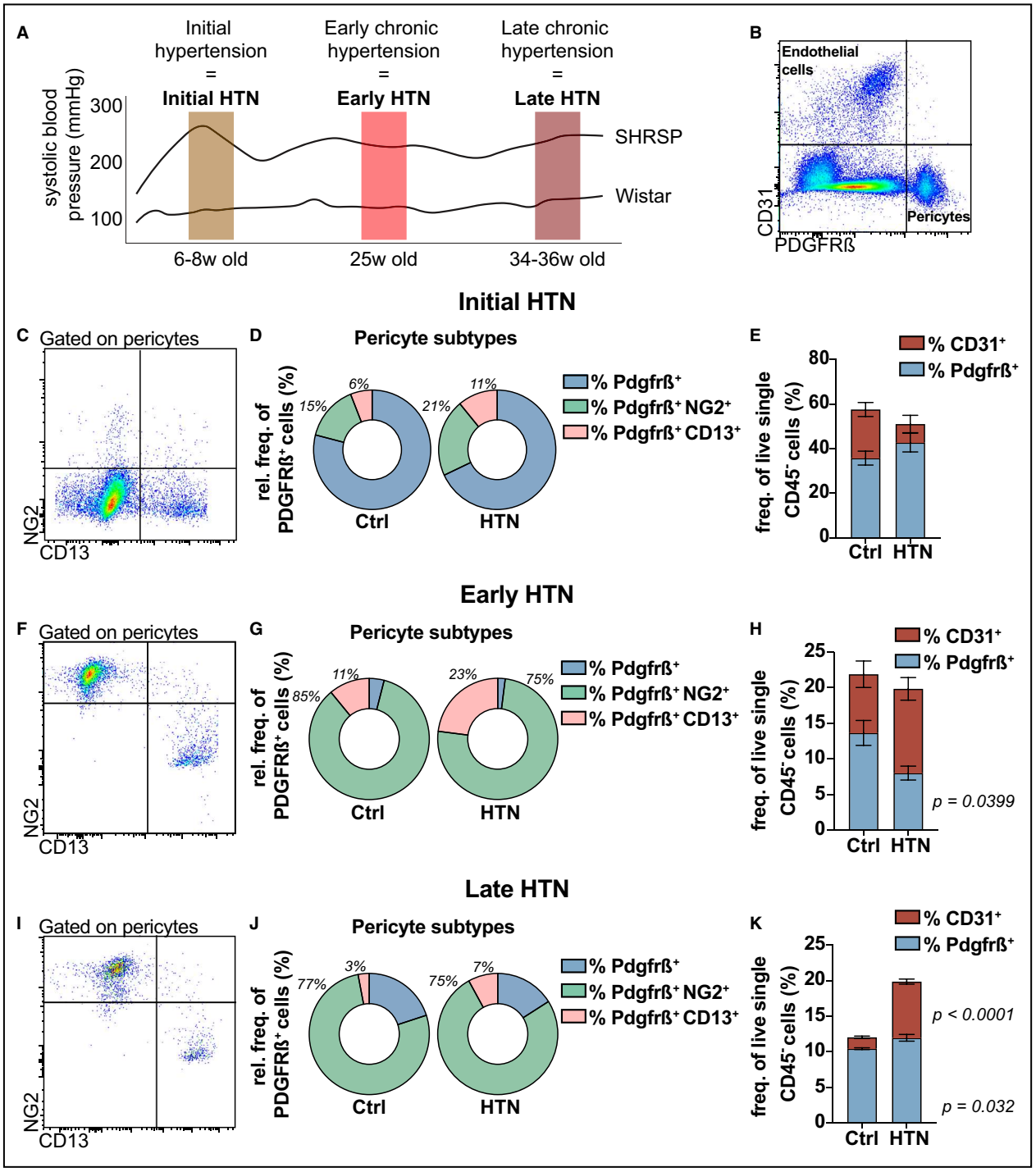

Figure 1. Progressive phenotypic shifts in brain pericytes across arterial hypertensive states.
Systolic blood pressure depiction across 3 hypertension phases in SHRSPs and Wistar rats. (**A**) Systolic blood pressure (mm Hg) in SHRSPs demonstrate increasing hypertension from initial hypertension (6–8 weeks), early chronic hypertension (25 weeks), and late chronic hypertension (34–36 weeks) phases, with Wistar rats as controls. Age of rats at each time point is shown on the *x* axis. Blood pressure trends are representative, detailed in Figure S1. (**B**) Gating strategy employed to select live vascular cells, excluding CD45 cells, and subsequent identification of CD31$^+$ endothelial cells and PDGFRß$^+$ pericytes. (**C** through **K**) Pericyte subtype identification across hypertension phases: initial hypertension (**C** through **E**), early chronic hypertension (**F** through **H**), and late chronic hypertension (**I** through **K**). Differential expression of NG2 and CD13 among PDGFRß$^+$ pericytes is depicted (**D**, **G**, **J**), alongside relative frequencies and comparisons of endothelial and pericyte populations (**E**, **H**, **K**). For experimental methodology see Figure S2A and S2B. n=6 per group for initial and early chronic hypertension, n=5 per group for late chronic hypertension; experiments were performed twice per group per time point. Data are presented as mean±SEM. CD indicates cluster of differentiation; HTN, hypertension; NG2, neuroglial antigen 2; PDGFRß, platelet-derived growth factor receptor ß; and SHRSP, spontaneously hypertensive stroke-prone rat.

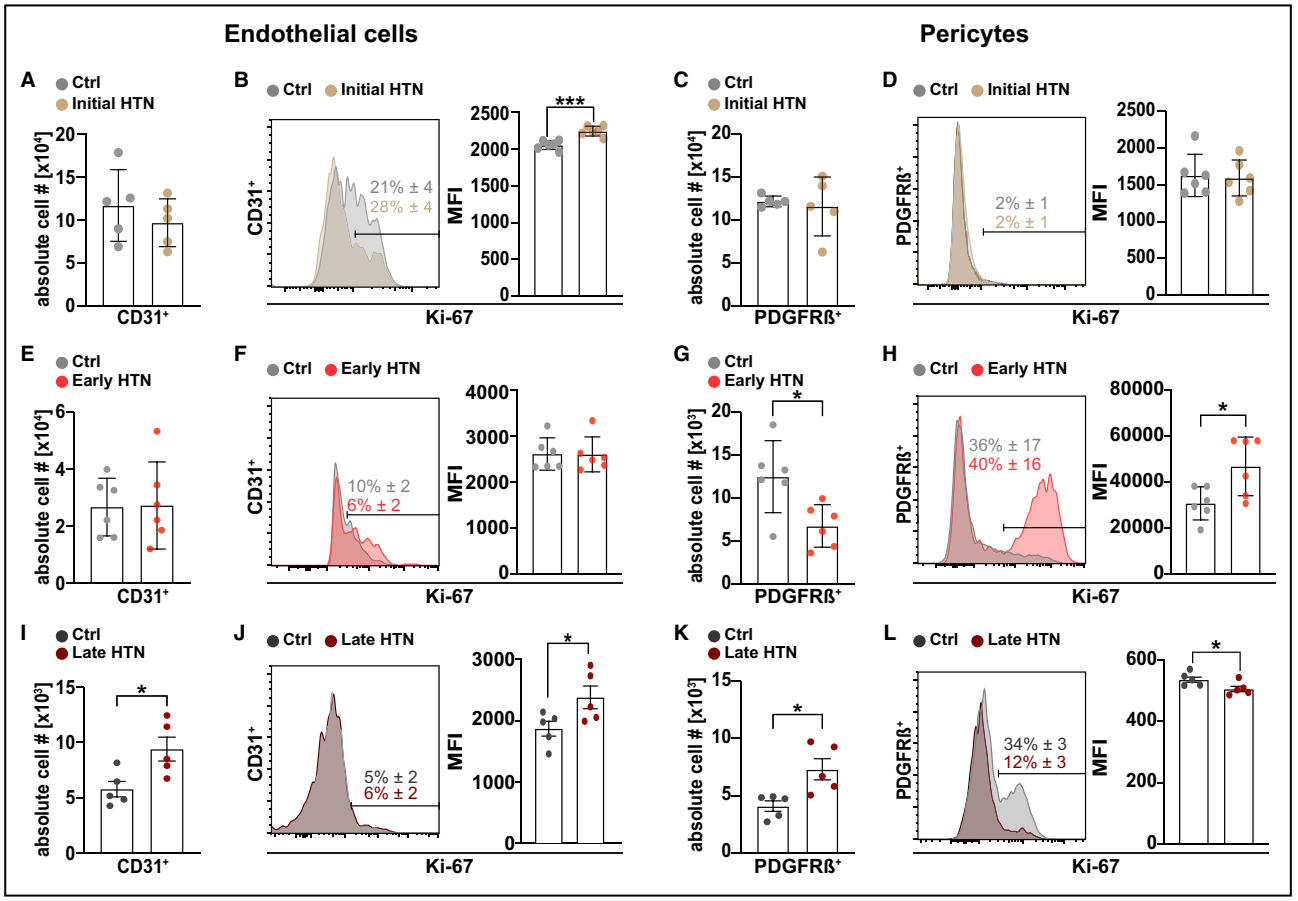

Figure 2. Vascular cell abundance and proliferation across hypertension stages.
Analysis of endothelial cells and pericytes abundance across hypertension stages. Row-wise representation of initial hypertension (**A** through **D**), early chronic hypertension (**E** through **H**), and late chronic hypertension phases (**I** through **L**), detailing absolute numbers of PDGFRß⁺ pericytes and CD31⁺ endothelial cells comparing control (control) vs hypertensive groups. Histograms and bar graphs represent Ki-67 expression and quantification of CD31⁺ and PDGFRß⁺ cells. For experimental methodology see Figure S2a. Each data point represents 1 biological sample, experiments were performed twice per group and time point. Data are presented as mean±SEM. **P*<0.05, ****P*<0.001. CD indicates cluster of differentiation; HTN, hypertension; Ki-67, antigen Kiel 67; MFI, mean fluorescence intensity; and PDGFRß, platelet-derived growth factor receptor ß.

and identifying subclusters expressing NG2 and CD13, which point to the intricate interplay within the vascular cell milieu. Normalizing mean fluorescence intensity to the initial control expression levels of CD31, PDGFRß, NG2, and CD13 allowed us to trace the marker expression trajectory throughout hypertension development (Figure 3C). Initial and late chronic hypertension stages exhibit elevated CD31 expression showing an endothelial component reacting to hypertensive conditions. Conversely, PDGFRß expression peaked in initial controls, while NG2 and CD13 expressions dominated the hypertensive groups, especially in the chronic phases. Finally, we aimed to encapsulate the spatial and temporal shifts in marker expression profiles to provide a clear visual narrative of each individual marker over time. Our results showed the phenotypic shift in critical vascular markers, illustrating the complex development of vascular identity under the influence of hypertension (Figure 3D).

Molecular Pathways Underlying Hypertension-Induced Vascular Remodeling

To pinpoint the molecular basis of vascular remodeling in hypertension, we conducted an in-depth analysis of isolated microvessels using a custom polymerase chain reaction array focusing on genes within key pathways pivotal to understanding the vascular consequences of chronic hypertensive states—angiogenesis, BBB integrity, hypoxia, inflammation, and specific pericyte markers. This targeted analysis aimed to link transcriptional changes that accompany and possibly precipitate the vascular alterations seen in hypertension. Our results revealed the microvessel transcriptional landscape, pinpointing genes that undergo significant regulation in response to hypertensive stress. In the early chronic phase (Figure 4A), a notable upregulation of 31 genes (fold change >1.5, *P*<0.05), including

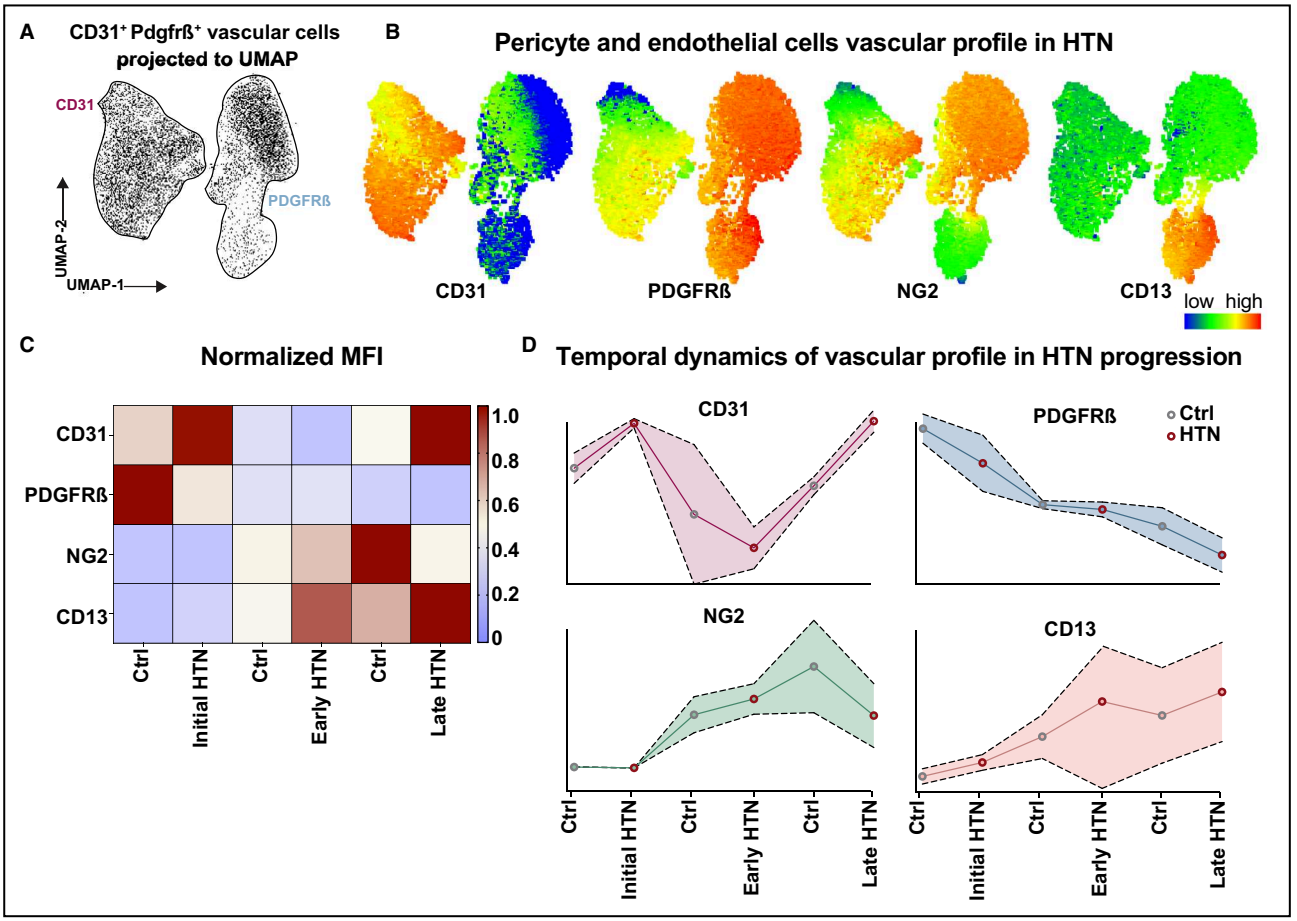

Figure 3. Temporal dynamics of vascular cell marker expression across hypertension progression.
UMAP visualization of vascular cell heterogeneity and expression patterns. (**A**) UMAP projection of CD31⁺ and PDGFRß⁺ cells. (**B**) Representative expression heatmaps of CD31, PDGFRß, NG2, and CD13 within the vascular clusters to depict overlapping expression of investigated pericyte markers. (**C**) Heat map of vascular cell expression levels of CD31, PDGFRß, NG2, and CD13 across 6 groups: initial control, initial hypertension, early chronic control, early chronic hypertension, late chronic control, and late chronic hypertension, from 2 independent experiments per time point, shown as normalized MFI values to the expression levels of the initial control group. For experimental methodology see Figure S2A and S2B. (**D**) Line graphs displaying the temporal progression of marker expression for CD31, PDGFRß, NG2, and CD13, individually across all examined time points. CD indicates cluster of differentiation; HTN, hypertension; MFI, mean fluorescence intensity; NG2, neuroglial antigen 2; PDGFRß, platelet-derived growth factor receptor ß; and UMAP, uniform manifold approximation and projection.

Agtr1a, Epas1, Timp3, Tek, Notch3, Vegfb, and *Mmp9*, displayed a state of heightened vascular reactivity and remodeling. Inflammatory vascular processes were displayed by the upregulation of *TNF, Icam1, Ccl2, Ccl5, IL10, Il1b, Ifng, Bdkrb1*, and *Nos2* (Figure 4A and 4E). On the other hand, in late chronic hypertension, 35 genes were downregulated (Figure 4B and 4E). This difference displays the specific effects of hypertension on vascular gene expression, demonstrating the progression from an active transcriptional response in the early phase to a more subdued profile in late chronic hypertension. To examine these transcriptional shifts, we further dissected the expression patterns of each gene relative to their levels in the early hypertension control group (Figure S3). These analyzed genes were specifically selected for the custom polymerase chain reaction array because they represent key molecular pathways underlying hypertension-induced vascular remodeling. These pathways include hypertension/hypoxia (Figure S3A), specific pericyte markers (Figure S3B), angiogenesis/blood–brain barrier (Figure S3C), and inflammation (Figure S3D).

Next, we examined the biological pathways that were prominent in the observed transcriptional changes. Our findings revealed that early chronic hypertension is a phase marked by active vascular transformation, with upregulated genes indicating a substantial role of the vasculature in processes including blood flow regulation, lipid response, blood pressure control, angiogenesis, and inflammation (Figure 4c). The late chronic hypertension phase revealed a decrease in the activity of pathways, which may indicate a decline in the ability

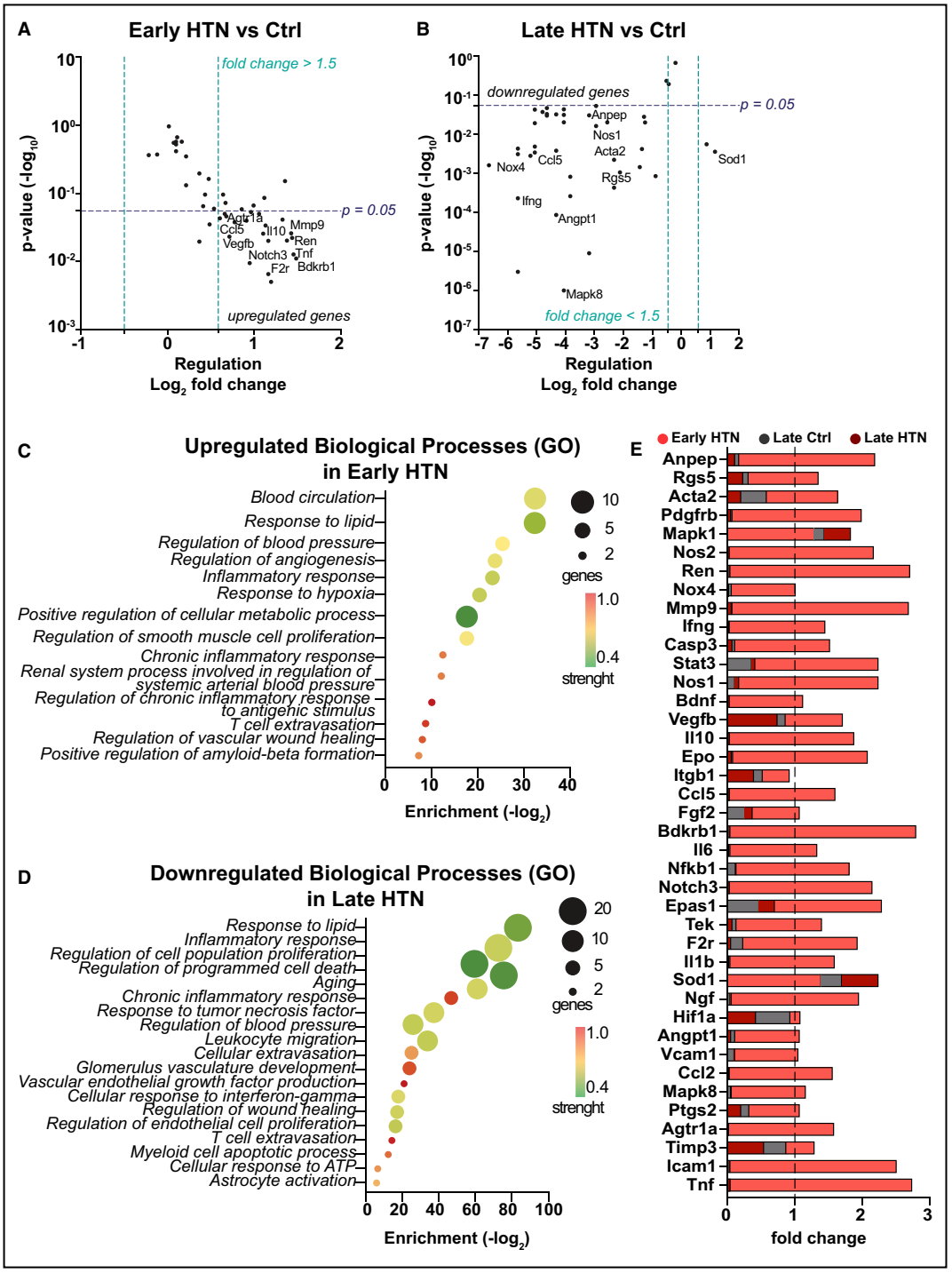

Figure 4. Microvessel-based changes in lipid, angiogenic, and inflammatory pathways during the progression of hypertension.

Microvessel isolation methodologies are detailed in Figure S2C. (**A**) Volcano plot displaying the differential gene expression between control and early chronic hypertensive pericytes. Each dot represents 1 gene. The vertical green dotted lines indicate the 1.5-fold change threshold beyond which gene expression differences are considered potentially biologically significant. The horizontal blue dotted line indicates the statistical significance threshold (P<0.05) dividing genes with significant expression changes from those without. (**B**) Volcano plot for late chronic hypertensive state. (**C, D**) GO and reactome pathway analyses displaying the upregulated biological processes in early chronic hypertension and downregulated processes in late chronic hypertension. (**E**) Side bars representative of individual gene expression levels between early and late chronic hypertensive states against early control. Relative gene expression levels were normalized to *Hprt* and further normalized to the average expression of early control (dotted line); exact P values are provided in Figure S3. Ctrl indicates control; GO, gene ontology; and HTN, hypertension.

of blood vessels to adapt to high blood pressure and a potential failure to respond to the hypertensive challenge, characterized by a reduction in the expression of genes involved in lipid metabolism, inflammation, cell proliferation, and programmed cell death (Figure 4D).

In Vitro Pericyte Expression Dynamics Mirror In Vivo Findings, Showing Hypertension-Driven Reductions in PDGFRß Alongside Elevations in NG2 and CD13

Following the characterization of vascular cell dynamics across chronic hypertensive stages, we shifted our attention to a carefully controlled in vitro setting to gain a deeper understanding of the effects of hypertensive stress on pericyte behavior (Figure 5). Our in vitro approach began with the isolation of microvascular fragments, their seeding, expansion, and precise pericyte enrichment, free from endothelial cell influence (Figure S4).[44] Immunofluorescence analyses confirmed the specificity and integrity of our pericyte cultures through PDGFRß expression and paralleled the significant shifts observed in ex vivo pericyte marker expression in response to early chronic hypertension. In vitro analysis distinctly demonstrated that PDGFRß$^+$ pericytes derived from early chronic hypertensive states exhibited a significant upregulation of both NG2 and CD13, with a particularly pronounced increase in CD13 expression compared with controls. Conversely, PDGFRß$^+$ pericytes from age-matched controls displayed NG2 expression but only a slight increase in CD13, maintaining a robust PDGFRß expression (Figure 5A and 5B). Quantitative flow cytometric analysis further validated these observations, revealing significant phenotypic alterations in hypertensive pericytes, particularly in the expression patterns of PDGFRß, NG2, and CD13 (Figure 5C through 5G). The significant rise of CD13$^+$ pericytes in the hypertensive group contrasts with the more moderate changes seen in control pericytes, reinforcing our characterization of the dynamic response of pericytes to hypertensive and environmental stress.

EV-Mediated Recovery of Mitochondrial Function in Hypertensive Pericytes

Expanding on our initial in vitro research on pericyte adaptation, we extended our investigation to explore the therapeutic potential of pdEVs on pericyte mitochondrial function under hypertensive conditions. This aspect is critical for maintaining cellular health and vascular integrity during stressful conditions[50] (Figure 6). Our experimental strategy involved isolating plasma and pdEVs (Figure S2E) from rodents during early chronic hypertension, a time point characterized by increased inflammatory, hypoxic, hypertensive, and BBB disruption markers (Figure S3). To specifically assess the impact of pdEVs, both plasma and enriched EV samples from hypertension and age-matched control rodents were used to stimulate pericytes, allowing us to differentiate the effects of pdEVs from those potentially contributed by other plasma components. Then, these biological nanoparticles were used to stimulate both normotensive and hypertensive pericytes in vitro, aiming to investigate the influence of circulating factors from this critical hypertension stage on mitochondrial function in vascular cells. This approach provides a direct assessment of the role of hypertensive pdEVs in mediating vascular changes, which may establish a crucial link between systemic hypertension and its impact on vascular cells.

Flow cytometric analysis confirmed the isolation of pdEVs,[48] with size gating and tetraspanin selection (CD9, CD63, and CD81), revealing no difference in abundance of circulating pdEVs between early chronic hypertension and age-matched control (Figure 6A and 6B). Using the JC-10 dye, which provides a quantifiable measure to assess mitochondrial membrane potential, we assessed the mitochondrial function in pericytes. In healthy cells with an intact mitochondrial membrane potential, JC-10 aggregates in the mitochondria, emitting red fluorescence (Figure 6C). However, when the mitochondrial membrane potential is compromised, JC-10 fails to aggregate and remains in its monomeric form, emitting green fluorescence.

Our findings reveal that hypertensive pdEVs induced significant mitochondrial depolarization in control pericytes, leading to a marked reduction in the JC-10 aggregate/monomer ratio, indicative of mitochondrial dysfunction (Figure 6D through 6F). This mitochondrial impairment was not only observed in control pericytes stimulated with hypertensive pdEVs but also inherently in unstimulated hypertensive pericytes, highlighting their baseline mitochondrial compromise (Figure 6f). Interestingly, the application of pdEVs derived from normotensive rodents to hypertensive pericytes demonstrated a significant recovery of mitochondrial function, as indicated by the restoration of the JC-10 aggregate/monomer ratio to normal levels.

Metabolic Reprogramming of Pericytes in Hypertension-Induced Vascular Cell Dysfunction

After uncovering the disruptions to mitochondrial function caused by hypertensive stimuli, we conducted further research on the metabolic characteristics of pericytes derived from hypertensive conditions. We aimed to dissect their broader metabolic response to hypertension-induced stress to capture the essence of their metabolic adaptability and resilience (Figure 7). Therefore, we conducted an extensive metabolic profile

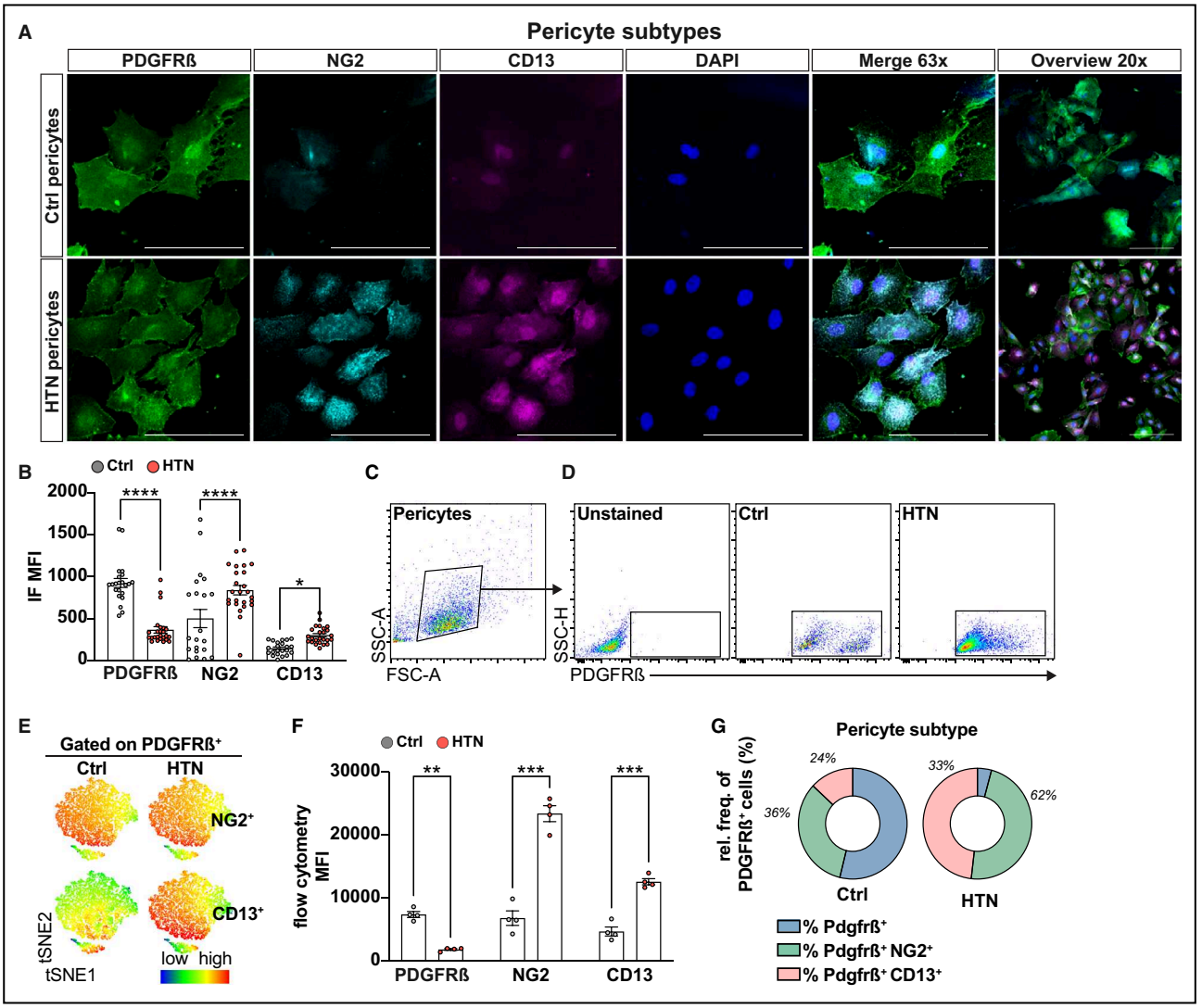

Figure 5. Pericyte expression dynamics revealed a hypertension-driven reduction in PDGFRß and boost in NG2 and CD13 expression.

(**A**) Immunofluorescence imaging analysis for pericyte subtype identification in cultures, revealing differential expression of PDGFRß, NG2, and CD13 across control and hypertensive pericytes. Images show 63x high-resolution merges and a 20× overview of pericyte subtype distribution. (**B**) Quantitative analysis of MFI for PDGFRß, NG2, and CD13; each dot represents the average MFI measurements obtained per field of view. (**C** through **F**) Flow cytometric analysis and tSNE plots elaborating further on pericyte subtype characterization in vitro. Initial gating strategies are depicted to validate the expression of PDGFRß in all cells, followed by detailed analysis of NG2 and CD13 expression across pericyte populations using subsequent tSNE visualization and quantification; each dot represents the aggregate data of averaged duplicates derived from in vitro expansion that correspond to n=10 biological samples per group. (**G**) Relative frequencies of PDGFRß$^+$ cells displaying subtype distinctions within control and hypertensive groups in vitro derived from flow cytometric data. Microvessel isolation and pericyte enrichment methodologies are detailed in Figure S2C and S2D. Data are presented as mean ± SEM. $^{**}P<0.01$, $^{***}P<0.001$, $^{****}P<0.0001$. All scale bars represent 100 μm. CD indicates cluster of differentiation; HTN, hypertension; MFI, mean fluorescence intensity; NG2, neuroglial antigen 2; PDGFRß, platelet-derived growth factor receptor ß; and tSNE, t-distributed stochastic neighbor embedding.

analysis that examined oxidative phosphorylation and glycolysis in pericytes isolated from initial and chronic stages of hypertension. This approach was predicated on the hypothesis that hypertension has distinct effects on pericyte metabolism throughout its progression, potentially revealing metabolic vulnerabilities or adaptations unique to hypertensive vascular pathology (Figure 7A through 7C, Figure S2F).

Our analyses revealed a pronounced decline in maximal respiration capacity in chronic hypertensive pericytes, apart from their initial hypertensive counterparts (Figure 7D and 7E), indicating the progressive impairment of mitochondrial function as hypertension advances. Moreover, evaluation of the spare respiratory capacity, which assesses the potential of cells to respond to bioenergetic stress, showed a significant decrease in chronic

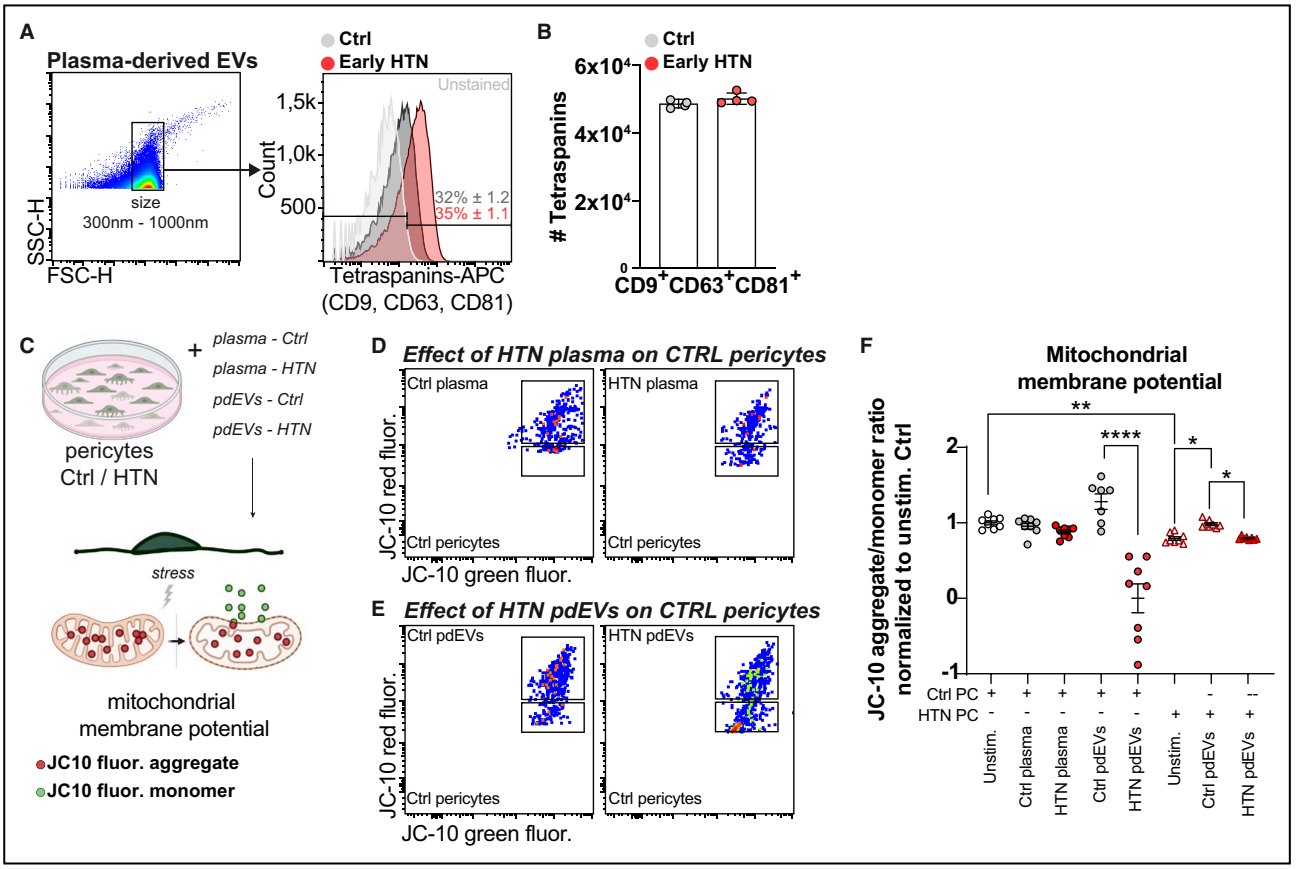

Figure 6. Hypertensive-derived extracellular vesicles cause selective mitochondrial disruption in control pericytes. pdEVs isolation methodologies are detailed in Figure S2E.

(**A**) Flow cytometric analysis displaying EV selection based on size gates using 300- to 1000-nm silica beads, followed by histograms indicating the counts, frequencies, and positive selection of tetraspanins (CD9, CD63, CD81). (**B**) Bar graphs comparing the absolute numbers of isolated pdEVs from control and hypertensive rodents. Each data point represents aggregate data of duplicates derived from 1 biological sample; experiment was repeated once. (**C**) Depiction of in vitro stimulation conditions with control pericytes derived from 6-wk-old rodents exposed to plasma or pdEVs derived from early chronic hypertension and age-matched control illustrating the experimental approach using JC-10 staining to assess the impact of hypertensive circulating factors on pericyte mitochondrial function. (**D**) Flow cytometric plots showing JC-10 fluorescence in control pericytes stimulated with plasma derived from control or hypertension. (**E**) Flow cytometric plots showing JC-10 fluorescence in control pericytes stimulated with pdEVs derived from control or hypertension. (**F**) Dot plot graph representing the JC-10 aggregate/monomer ratio in control (control) and hypertensive pericytes under various stimulation conditions. The data are normalized to unstimulated normotensive pericytes. Each data point represents aggregate data derived from 10 biological samples measured in duplicates and conducted twice. Data are presented as mean±SEM. **P*<0.05, ***P*<0.01, *****P*<0.0001. Ctrl indicates control; EV, extracellular vesicle; HTN, hypertension; and pdEVs, plasma-derived extracellular vesicles.

hypertension (Figure 7E). The assessment of ATP linked to mitochondrial activity showed a significant decrease in ATP production in pericytes from chronic hypertension as compared with both their initial hypertensive counterparts and age-matched controls. This decrease indicates a reduced efficiency of the mitochondria and illustrates a changing energy landscape, where the dependence on ATP synthesis by mitochondria decreases in the presence of hypertensive states (Figure 7E). Finally, the notable reduction in nonmitochondrial oxygen consumption rates in chronic hypertensive pericytes showed that the metabolic decline extends beyond mitochondrial function and indicates a general deterioration in cellular metabolic health (Figure 7E).

Following the sequential additions of glucose, oligomycin, and 2-deoxyglucose, we analyzed the extracellular acidification rate over time to observe the fluctuating patterns of glycolysis in pericytes. Both initial and chronic hypertensive pericytes exhibited significantly higher ATP production via glycolysis, as evidenced by increased extracellular acidification rate levels (Figure 7F). This indicates a metabolic shift toward glycolysis in the hypertensive state. The glycolytic capacity (Figure 7G), reflecting the maximum rate of glycolysis under stressed conditions, was significantly higher in hypertensive pericytes across both stages, emphasizing enhanced glycolytic dependence as a key feature of pericyte metabolic adaptation to hypertension.

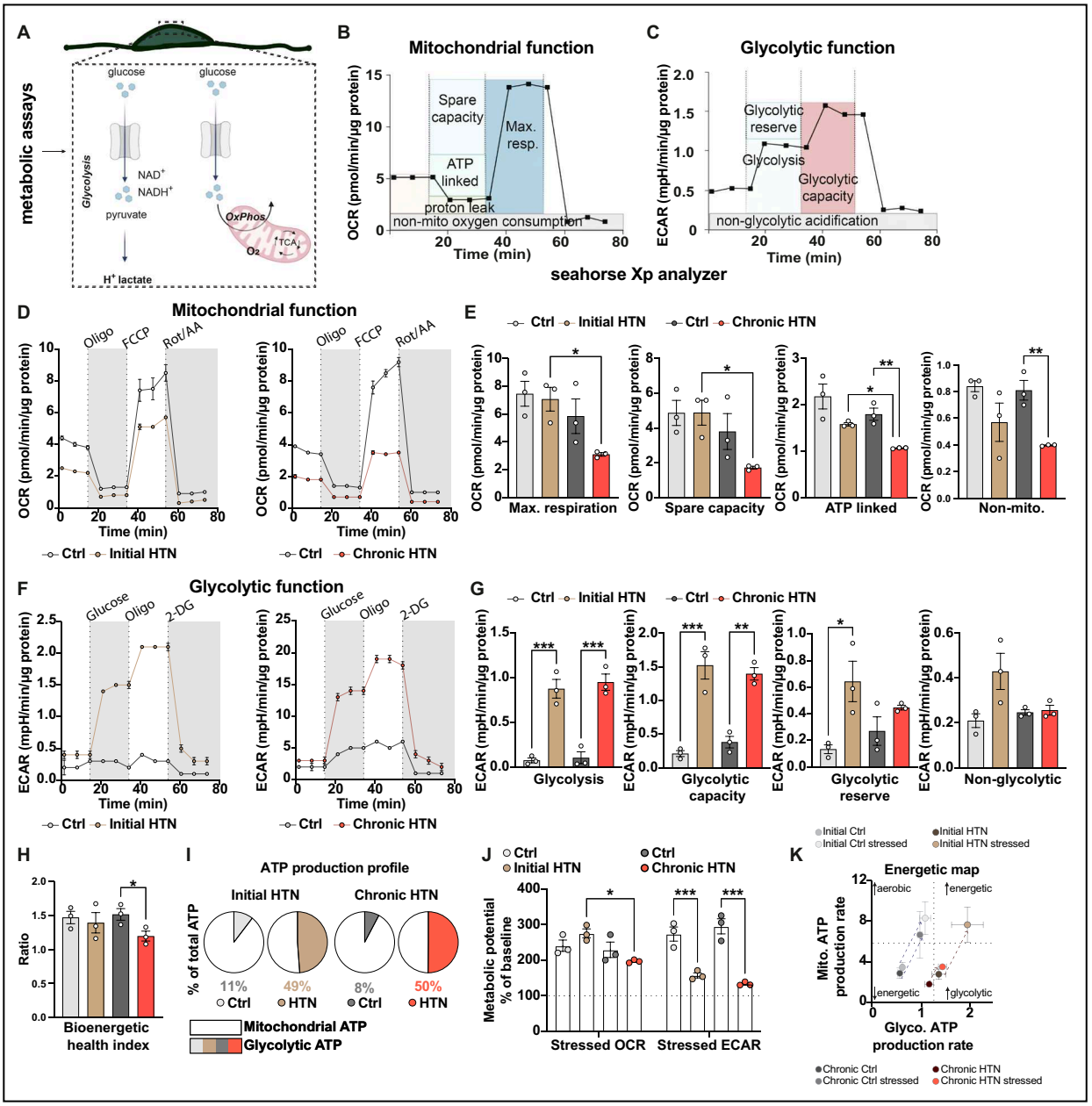

Figure 7. Bioenergetic reprogramming in pericytes upon hypertensive states.

(**A**) Schematic representation of the metabolic pathways analyzed in expanded pericyte cultures from different hypertension phases (Figure S2C and S2F). (**B**) Schematic overview of Seahorse extracellular flux analysis measured by mitochondrial stress test in pericytes, highlighting the steps involved in measuring OCR and (**C**) ECAR. (**D**) Analyses of OCR in pericytes of initial hypertension, chronic hypertension, and age-matched controls (n=8–10 per group) using a Seahorse extracellular flux analyzer. Dotted lines indicate the period and time of Oligo, FCCP, ROT, and Ant treatment. (**E**) Bar graphs depicting the maximal respiration capacity, spare capacity, ATP production linked to mitochondrial activity and non-mitochondrial OCR across control and hypertensive pericytes. (**F**) Visualization of glycolytic capacity and reserve in control and hypertensive pericytes. Dot lines indicate the period and time of glucose, Oligo, and 2-DG addition. (**G**) Bar graphs depicting glycolytic capacity, glycolytic reserve, and nonglycolytic ATP production. (**H**) Bar graph representing the Bioenergetic Health Index as a dynamic measurement of the pericyte response to stress. (**I**) ATP production profiles in control and hypertensive pericytes displaying the relative contribution of glycolysis and mitochondrial respiration to cellular ATP production. (**J**) Metabolic potential % of baseline showing the metabolic flexibility and potential of control and hypertensive pericytes under stress conditions. (**K**) Energetic map highlighting the metabolic shift in pericytes indicated by the contribution of glycolysis and mitochondrial respiration to ATP production under control and hypertensive conditions. Bar graphs represent mean±SEM of 3 independent experiments per group per time point, with each experiment including triplicates. Each data point represent aggregate data from initial groups (control and hypertension) derived from 8 biological samples each, and chronic groups (control and hypertension) from 10 biological samples each. Data are presented as mean±SEM *P<0.05, **P<0.01, ***P<0.001. 2-DG indicates 2-Deoxy-D-glucose; Ant, antimycin; Ctrl, control; ECAR, extracellular acidification rate; FCCP, carbonyl cyanide-p-trif luoromethoxyphenylhydrazone; HTN, hypertension; OCR, oxygen consumption rate; Oligo, oligomycin; and ROT, rotenone.

Interestingly, the glycolytic reserve (Figure 7G), which indicates the extent to which cells can further increase glycolysis from their baseline level, showed a significant increase in initial hypertensive pericytes compared with controls. However, this distinction did not persist in chronic hypertension, which represent a potential metabolic limit or saturation in further upregulating glycolysis as the disease progresses. The Bioenergetic Health Index provided a thorough evaluation of the metabolic health of pericytes, revealing a significant decrease in bioenergetic function in chronic hypertensive pericytes. This index emphasizes the negative impact of hypertension on pericyte metabolic capacity (Figure 7H).

Extending beyond oxidative phosphorylation and glycolysis measurements, our results revealed a striking shift in ATP production (Figure 7I). Initial hypertensive pericytes differed significantly from their control counterparts by generating a substantial portion of their ATP through glycolysis, as opposed to control pericytes (49% versus 11%). This striking shift persisted in chronic hypertension (50% versus 8%). These results show a metabolic shift in hypertensive pericytes, predisposing them to rely more heavily on glycolysis from the onset of the disease. The assessment of metabolic potential under stress conditions validated the influence of hypertension on pericyte energy dynamics (Figure 7J). Chronic hypertensive pericytes demonstrated a substantially reduced metabolic capacity compared with their initial hypertensive counterparts, implying a limited ability to fulfill increased energy demands or recover from stress. This compromised state was also apparent when contrasting extracellular acidification rate levels during stress, showing that both initial and chronic hypertensive pericytes were less capable of enhancing glycolysis in response to stress than controls, which revealed a vulnerability in their metabolic response mechanisms. The energetic map illustrates the metabolic states of pericytes across various conditions (Figure 7K). This visualization emphasizes that initial hypertensive pericytes are primarily glycolytic and exhibit heightened energetic responses when stressed, propelling them into a high-energy production state. In contrast, their control counterparts maintained aerobic profiles under stress conditions.

Given the crucial role of metabolic flexibility in preserving cellular and vascular health under hypertensive stress, we further investigated the consequences of metabolic inhibitors on ATP production in pericytes (Figure 8, Figure S5). Using mitochondrial inhibitors such as UK5099, etomoxir, and BPTES, we investigated the dependency of pericytes on ATP production pathways derived from mitochondria (Figure 8A). This resulted in a decrease in spare and maximum respiratory capacity in both control and hypertensive pericytes (Figure S5A through D), indicating successful mitochondrial pathway inhibition.

In control pericytes, the innate preference for mitochondrial ATP (oxidative phosphorylation) as the primary ATP production pathway displayed metabolic efficiency and flexibility. In response to mitochondrial inhibitors, these cells effectively increased glycolysis, highlighting their ability to adjust their energy production methods swiftly in response to bioenergetic stressors. Our results showed that control pericytes exhibit an aerobic profile evidence by their reliance on mitochondrial ATP under steady conditions, yet displaying an inherent capacity to engage glycolysis when necessary (Figure 8C and 8D; Figure S5E through S5H).

Considering that hypertensive pericytes rely on glycolysis as their primary energy source, we sought to reduce their primary energy production pathway using 2-deoxyglucose, a glycolysis inhibitor (Figure 8B). Hypertensive pericytes exhibited a greater dependency on glycolysis for ATP production, even before being subjected to the same mitochondrial constraints. Inhibition of glycolysis with 2-deoxyglucose presented a significant bioenergetic challenge, as evidenced by a substantial reduction in total ATP production (Figure 8E and 8F, Figure S5K). Although these cells have the potential to shift toward oxidative phosphorylation, the transition does not fully compensate for glycolytic blockade, highlighting a critical metabolic inflexibility. This observation is crucial, especially considering that initial hypertensive pericytes possess the mitochondrial machinery capable of ATP production, yet they display a marked preference for glycolysis (Figure S5I through S5L). Upon glycolysis inhibition, chronic hypertensive pericytes exhibited reduced glycolytic and limited mitochondrial ATP production, displaying an entrenched metabolic programming that favors glycolysis despite the availability of mitochondrial pathways.

DISCUSSION

In the field of brain vascular biology, our understanding of hypertensive vascular pathology has advanced significantly; however, the phenotypic and metabolic mechanisms of such changes, particularly at the level of cerebral pericytes, remain underexplored. Our in vivo and in vitro studies have demonstrated significant phenotypic changes in pericytes under hypertensive conditions, characterized by increased coexpression of NG2 and CD13, indicative of a stressed vascular phenotype adapting to ongoing hypertensive insult. These cellular transformations correlate with a profound metabolic reprogramming where pericytes shift toward a glycolysis-dominant metabolism already in the initial phase of hypertension emphasizing a paradigm shift in the metabolic programming of brain pericytes, which, although energy efficient under hypoxic

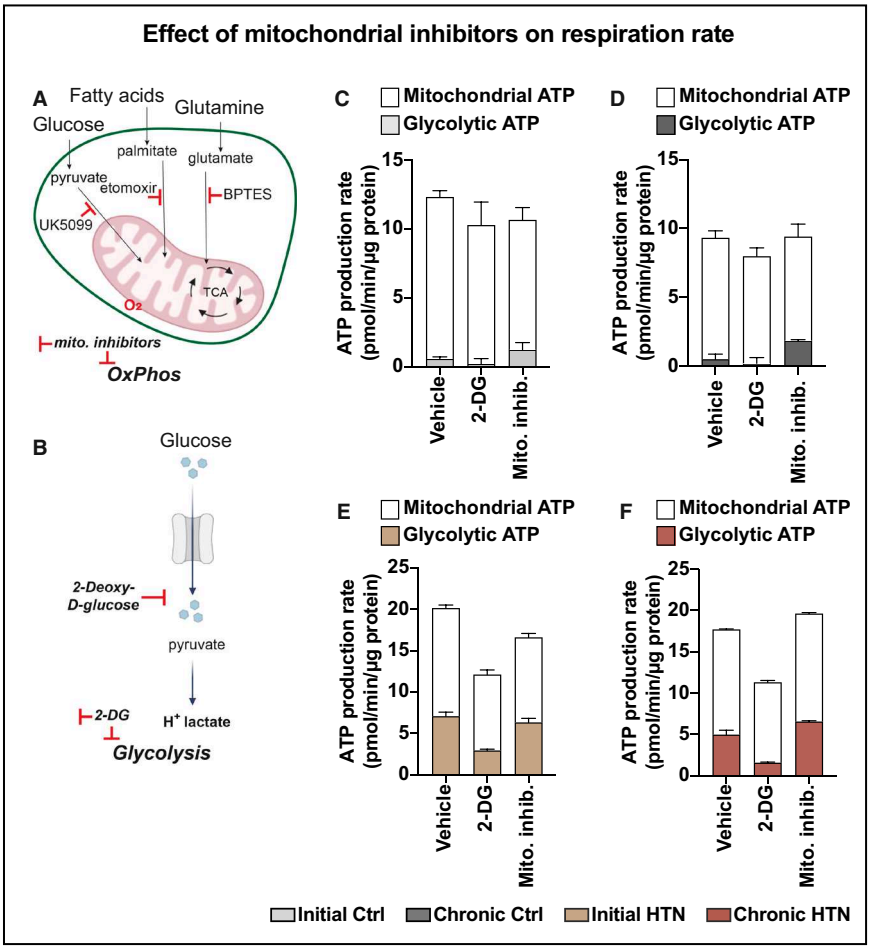

Figure 8. Effect of metabolic inhibition on ATP production in hypertensive and control pericytes.
(**A**) Schematic representation of the application of mitochondrial inhibitors (UK5099, etomoxir, BPTES) to delineate pathways leading to ATP production via mitochondrial oxidative phosphorylation in pericytes. (**B**) Schematic representation of glycolysis inhibition using 2-DG to block hexokinase. (**C, D**) Bar graphs representing total ATP production rates measured in control pericytes showing a predominant dependence on mitochondrial ATP. (**E, F**) Bar graphs representing total ATP production rate analysis in hypertensive pericytes demonstrating a continued preference for glycolysis. Measurements were performed in triplicate for each group at each time point, with initial groups (control and hypertension) derived from 8 biological samples each, and chronic groups (control and hypertension) from 10 each. 2-DG indicates 2-deoxyglucose; Ctrl, control; and HTN, hypertension.

or stress conditions, delineates a form of metabolic inflexibility when faced with prolonged hypertensive insult. This shift is not merely a passive reaction to altered physiological conditions but a proactive adaptation that can profoundly influence vascular metabolism and function.[51,52]

Pericytes, traditionally recognized for their role in capillary blood flow regulation and BBB integrity,[7,16,20] emerged from our study as central players in the metabolic reprogramming associated with hypertension. We detected already in the initial stages of hypertension a modest yet significant diversification in pericyte marker expression early on, with increases in NG2 and CD13 coexpression, indicating an early cellular response to rising blood pressure. Our findings revealed a critical transformation in pericyte phenotype, marked by upregulation of NG2 and CD13 and concurrent downregulation of PDGFRß. After central nervous system injury, NG2-reactive pericytes can be found near microvessels,[13] where they function as inflammation sensors and assist with immunosurveillance and effector functions of extravasated neutrophils and macrophages. These findings imply that NG2 may play a role in central nervous system injury that is linked to inflammation. It seems probable that NG2 also plays a role in the development of cSVD, which is characterized by increased BBB permeability, inflammatory infiltrates, and central nervous system

damage.[29] Increased expression of CD13 is a hallmark of an inflammatory response as it facilitates monocyte and endothelial cell adhesion, which is a critical event in the progression of vascular diseases.[53] This finding is consistent with literature showing that CD13 plays a pivotal role in inflammation and vascular remodeling.[53,54] Specifically, CD13 functions as a mediator of monocyte adhesion to endothelial cells,[54] potentially contributing to the inflammatory environment associated with cSVD. These results indicate a phenotypical pericyte shift from its typical functions toward a phenotype that is prepared for acute stress response and tissue repair. Interestingly, the distinct expression of these markers highlights a specific involvement of NG2 and CD13 in disease-specific vascular remodeling processes. NG2 acts as a general stress response marker, with its increased expression occurring in both normal and hypertensive conditions, whereas the upregulation of CD13 under hypertensive stress emphasizes its role in severe vascular responses, potentially leading to pathological changes.

The gene expression profile of microvessels across various stages of hypertension demonstrates a complex interplay of mechanisms that drive vascular pathology in chronic hypertension. The early stage of chronic hypertension was characterized by an upregulation of genes involved in lipid metabolism, angiogenesis, and inflammatory responses, suggesting an active process of vascular remodeling. Key genes, such as *Agtr1a, Ren*, and *acta2*, enhance systemic blood pressure regulation through their roles in the renin–angiotensin system, directly affecting pericyte contractility and vascular tone. Specifically, the *Agtr1a* gene encodes the angiotensin II type 1A receptor, which is essential for vascular and hemodynamic responses to angiotensin II. Studies have demonstrated that targeting this receptor leads to decreased blood pressure, reduced vascular tone responses, and significantly extends the life span of mice.[55–57] Renin, encoded by the *Ren* gene, catalyzes the conversion of angiotensinogen to angiotensin I, which is a crucial step in the renin–angiotensin–aldosterone system that influences fluid balance and vascular tone both vital for the regulation of blood pressure.[58] Furthermore, α-smooth muscle actin, encoded by the *Acta2* gene, plays a crucial role in the contractile function of vascular smooth muscle cells and pericytes. In conditions such as pulmonary hypertension *Acta2*-expressing pericytes undergo expansion and partial smooth muscle cell differentiation, contributing to arteriolar muscularization.[59] This leads to dysregulated signaling pathways that favor endothelial cell activation and inflammation.[59] The activation of the renin–angiotensin system at the early chronic hypertension stage highlights the crucial function of these genes in regulating vascular responses and preserving vascular integrity amid hypertensive conditions.

Similarly, *Notch3* supports the restructuring of vascular architecture by influencing both pericyte function and endothelial cell interactions essential for adapting to increased hypertensive stress and maintaining vascular integrity.[60,61] Protease-activated receptor 1, encoded by the *F2r* gene, plays a crucial role in vascular homeostasis, inflammation, and thrombosis, all of which are essential processes in vascular remodeling and the response to hypertension.[62] Parallel to these regulatory genes, a significant vascular inflammatory response was evident from the upregulation of *Tnf, Ccl2, Ccl5, Il1b, Il6, Ifng*, and *Nos2*, genes that orchestrate a robust immune response by mobilizing immune cells, exacerbate vascular inflammation and contribute to atherosclerotic lesion formation.[63–68] With the surge in *Ccl5*, an upregulation of *Il10* was detected, which may potentially serve as a compensatory mechanism to mitigate excessive inflammatory damage and preserve vascular function. This is because interleukin-10 has been shown to exert an upregulatory effect on the antihypertensive activity of chemokine (C-C motif) ligand 5.[69] Structural remodeling can be additionally mediated by *Mmp9* and *Vegfb*. This interaction is vital for both physiological and pathological vascular responses,[70,71] as it plays a role in both normal and abnormal vessel growth. *Mmp9* is responsible for breaking down and reorganizing the extracellular matrix, which is essential for vascular repair, while *Vegfb* promotes pathological angiogenesis,[72] especially when vascular endothelial growth factor levels are elevated. This can lead to vascular damage and the growth of abnormal blood vessels, indicating an adaptive yet potentially harmful response.

As hypertension progresses to its late chronic phase, a significant shift occurs with a decline in the expression of many previously upregulated genes, which may suggest a possible exhaustion of metabolic and adaptive capacities. However, the significant upregulation of *Sod1* stands out. *Sod1*, plays a critical role in mitigating oxidative stress by catalyzing the dismutation of superoxide radicals into oxygen and hydrogen peroxide, and increased expression in the late chronic phase might indicate an elevated oxidative stress environment within vascular cells.[73] This adaptive response could represent a mechanism to counteract increased oxidative damage associated with prolonged hypertension,[22] attempting to preserve cellular function and prevent oxidative injury.[74] Nonetheless, persistent high expression of *Sod1* might also reflect the chronic stress state of the vascular cells, potentially contributing further pathological changes if the oxidative burden overwhelms the cell's antioxidative capacities.

In our exploration of the systemic effects of hypertension on vascular cell biology, we observed profound alterations in mitochondrial function when control pericytes were exposed exclusively to plasma-derived EVs

from hypertensive rodents, without the influence of other soluble factors or cytokines. Our results demonstrate that circulating EVs within hypertensive states possess a specific ability to disrupt cellular bioenergetics beyond plasma interactions with primary vascular compartments. The observed decrease in mitochondrial membrane potential in response to hypertensive EVs, but not to plasma alone, indicates the potency and specificity of EVs as carriers of propathogenic signals. This depolarization suggests a direct detrimental effect of hypertensive pdEVs on mitochondrial integrity and function, compromising cellular energy production, indicating for the first time a novel pathway through which hypertension may exert vascular damage. These findings are particularly intriguing, given the established role of EVs in mediating cell-to-cell communication and their potential to carry a multitude of bioactive molecules, including inflammatory mediators, microRNAs, and other noncoding RNAs, which can profoundly influence recipient cell behavior.[31,32] The ability of hypertensive EVs to impair mitochondrial function in pericytes may reflect a mechanistic pathway through which hypertension inflicts systemic damage, leading to the disruption of vascular and potentially neurovascular functions. This interaction highlights the broader implications of our findings, linking localized vascular dysfunction to systemic vascular health. In the context of hypertension, where elevated systemic inflammatory markers are common,[22] the impact of circulating EVs becomes a critical factor in the perpetuation of vascular pathology.

However, against these detrimental impacts, our further analysis revealed a restorative potential of pdEVs sourced from normotensive controls. The use of these pdEVs resulted in a marked improvement in the mitochondrial membrane potential of hypertensive pericytes, indicating their ability to reverse the dysfunction caused by hypertension. This finding shows the potential of using pdEVs as a therapeutic strategy and suggests that modifying the vesicular cargo could pivot these vesicles from pathological contributors to beneficial agents in stabilizing vascular function under hypertensive conditions. Accordingly, while we have shown that pdEVs can transmit pathological effects, our findings elevate the discourse by demonstrating their therapeutic capacity dependent on their vesicular cargo. This indicates the critical need for future studies to dissect the specific contents of these EVs, determining how differences in cargo between healthy and diseased states may dictate their impact on vascular health. Such studies could pave the way for harnessing pdEVs not only as biomarkers but also as a dynamic agent in developing targeted interventions for hypertensive microvascular complications.

We further investigated the metabolic requirements of pericytes and observed that hypertensive pericytes undergo a shift toward a glycolytic phenotype to maintain the increased metabolic demands and mitigate oxidative stress, a strategy reminiscent of cancer cells.[75,76]

This glycolytic shift in hypertensive pericytes, akin to the Warburg effect observed in cancer cells, indicates that despite the availability of oxygen, pericytes opt for glycolysis, a less efficient pathway for ATP generation, to sustain vital functions under stress,[76,77] highlighting a potential metabolic adaptation that favors rapid response over efficiency, similar to the metabolic preference seen in proliferating cancer cells. This shift supports not only cellular survival but also vascular stability and neuronal health, particularly in situations of hypertension. However, unlike tumor cells, which leverage this metabolic shift to support rapid proliferation, pericytes in hypertensive states seem to mainly use glycolysis to sustain their vital functions under stress, thereby supporting vascular stability. This adaptation, while beneficial in the short term for cellular survival, may nevertheless lead to long-term cellular exhaustion and vascular dysfunction. The implications of these findings extend beyond mere cellular survival influencing the entire neurovascular unit, contributing to the inflammatory processes frequently observed in chronic hypertension. Pericytes, which are responsible for regulating cerebral blood flow, may lose their ability to do so effectively due to altered signaling pathways, including those mediated by nitric oxide and inflammatory mediators such as tumor necrosis factor-α and interleukin-6. As a result, the vascular dysfunction can exacerbate neuronal damage. The chronic activation of this inflammatory cascade disrupts not only pericytes but also endothelial cells and astrocytes, compounding the deleterious effects on cerebral homeostasis. The glycolytic shift in hypertensive pericytes is particularly evident in mitochondrial dysfunction, which becomes more pronounced in chronic hypertension. Despite their glycolytic bias, chronic hypertensive pericytes face limitations in enhancing their energy production under stress due to mitochondrial inefficiencies. This observation suggests that, at advanced disease stages, hypertensive pericytes operate near their maximal capacity, a critical state that risks compromising cellular integrity under prolonged or severe stress. Our data demonstrate that while early hypertensive pericytes retain some ability to utilize mitochondrial pathways, chronic conditions result in heavy reliance on glycolysis. However, this reliance on glycolysis can contribute to their susceptibility when faced with conditions that limit this energy pathway, indicating a significant shift away from the ability to adapt metabolically. This change in energy strategy points to an adjustment that, while initially compensatory, may become disadvantageous due to reduced mitochondrial function. The metabolic inflexibility of chronic hypertensive pericytes could be attributed to saturation

of mitochondrial capacity, where the demand for ATP and biosynthetic precursors exceeds the ability of mitochondria to function efficiently. This profound metabolic shift in pericytes may influence their interaction with other neurovascular unit components such as endothelial cells, neurons, microglia, and astrocytes, potentially exacerbating inflammatory responses and contributing to vascular leakage and BBB dysfunction.[29] The metabolic vulnerability of pericytes demonstrates a key aspect of hypertensive pathology and offers a novel target for therapeutic interventions.

In conclusion, our findings present an evaluation of the physiological and cellular strategies employed by vascular cells in response to chronic arterial hypertension, emphasizing significant phenotypic and metabolic transformations. By understanding and potentially manipulating these broad cellular responses, including metabolic pathways, particularly through targeted interventions that restore metabolic flexibility, some of the severe complications associated with chronic hypertension may be mitigated, and cognitive functions might be preserved. This approach could introduce a new era in the treatment of hypertensive vascular diseases, in which a holistic and metabolic modulation of vascular cells becomes a keystone of therapeutic strategies.

CONCLUSIONS

Our research demonstrates that cerebral pericytes in hypertensive conditions undergo phenotypic and metabolic changes, primarily shifting toward glycolysis in response to stress. Our results have shown pdEVs from hypertensive rodents significantly impair mitochondrial function in control pericytes, highlighting their role as biomarkers and as active agents in vascular pathology within the neurovascular unit. Importantly, our study demonstrates the therapeutic potential of pdEVs from normotensive control, which effectively restored mitochondrial function in hypertensive pericytes. This finding suggests that altering pdEV cargo can convert these EVs from disease agents to therapeutic tools, stabilizing vascular function under hypertensive stress. These results confirm the dual role of pdEVs in transmitting and mitigating vascular pathology, advocating for further investigation into their cargo to understand their therapeutic potential. This opens the possibility for innovative treatments targeting hypertensive vascular complications, using pdEVs both as precision biomarkers and as therapeutic agents in a individual approach.

Strengths and Limitations

Our study demonstrated metabolic reprogramming and phenotypic shifts of cerebral pericytes in response to chronic arterial hypertension; however, it is important to recognize certain limitations. The reliance on the SHRSP model, specifically selected for its human-like progression of hypertensive small-vessel disease, may not fully capture the complexity of human pathology due to species-specific differences. Male rats were chosen primarily due to their consistent and predictable hypertensive profile, which minimizes the variability associated with hormonal cycles in females, yet it restricts our understanding to only half of the potential patient population. We recommend that future studies should address this aspect to determine sex-dependent differences in the hypertensive response and pericyte behavior.

In terms of methodologies, our study heavily relied on flow cytometry to analyze phenotypic changes and quantify cell types and this technique inherently lacks the spatial context provided by histological analyses. Therefore, the interpretation of our flow cytometry results would benefit from orthogonal validation techniques such as immunohistochemistry or in situ hybridization. Additionally, while our approach evidences the role of metabolic shifts toward glycolysis in hypertensive pericytes, in vitro conditions may not entirely replicate an in vivo microenvironment because pericytes are maintained in ideal conditions, potentially oversimplifying the interaction dynamics between pericytes and other systemic, vascular, or neural components. Despite these limitations, our study advances our understanding of hypertensive vascular pathology by indicating how metabolic inflexibility and mitochondrial dysfunction in pericytes contribute to cerebrovascular disease progression. The contribution of our study is significant, offering novel insights into the pathophysiology of cSVD, and pointing to metabolic modulation as a promising therapeutic strategy.

ARTICLE INFORMATION

Received August 25, 2024; accepted November 19, 2024.

Affiliations

Medical Faculty, Institute of Inflammation and Neurodegeneration, Otto-von-Guericke University Magdeburg, Magdeburg, Germany (L.M., A.P.G., L.E.V., I.R.D.); Department of Neurology, Otto von Guericke University Magdeburg, Magdeburg, Germany (G.D., S.H., P.A., S.S.); German Center for Neurodegenerative Diseases (DZNE) within the Helmholtz Association, Magdeburg, Magdeburg, Germany (S.H., P.A., S.S.); Department of Neurology, Heinrich Heine University Düsseldorf, Düsseldorf, Germany (S.G.M.); Center for Behavioral Brain Sciences (CBBS), Magdeburg, Germany (S.S., I.R.D.); and German Center for Mental Health (DZPG) (S.S., I.R.D.), Center for Intervention and Research on Adaptive and Maladaptive Brain Circuits Underlying Mental Health, Halle-Jena-Magdeburg, Germany (C-I-R-C).

Acknowledgments

The authors thank Petra Grüneberg, Dr Abidat Schneider, and Cornelia Garz for their expert technical assistance. Figures 6C, 7A through C, 8A, and 8B and Figure S2A and S2C through F were created in BioRender (Biorender.com).

Author contributions: Drs Morton and Dunay conceptualized the study; Dr Morton designed experiments and methodology; Drs Morton, Garza, and Debska-Vielhaber conducted experiments and compiled the data with technical assistance provided by Drs Villafuerte, Henneicke., and Arndt; Drs Morton, Garza, and Debska-Vielhaber analyzed and interpreted

experimental data; Dr Morton created all figures and wrote the original draft of the manuscript;Drs Garza, Debska-Vielhaber, Villafuerte, Henneicke, Arndt, Meuth, Schreiber, and Dunay reviewed and edited the manuscript; Drs Schreiber and Dunay acquired all funding. All authors have read and agreed to the published version of the manuscript.

Sources of Funding

This study was supported by funds from the Deutsches Zentrum für Psychische Gesundheit—Center for Intervention and Research on Adaptive and Maladaptive Brain Circuits Underlying Mental Health.

Disclosures

None.

Supplemental Material

Tables S1–S3
Figures S1–S5

REFERENCES

1. Yang AC, Vest RT, Kern F, Lee DP, Agam M, Maat CA, Losada PM, Chen MB, Schaum N, Khoury N, et al. A human brain vascular atlas reveals diverse mediators of Alzheimer's risk. *Nature*. 2022;603:885–892. doi: 10.1038/s41586-021-04369-3
2. Obermeier B, Daneman R, Ransohoff RM. Development, maintenance and disruption of the blood-brain barrier. *Nat Med*. 2013;19:1584–1596. doi: 10.1038/nm.3407
3. Knox EG, Aburto MR, Clarke G, Cryan JF, O'Driscoll CM. The blood-brain barrier in aging and neurodegeneration. *Mol Psychiatry*. 2022;27:2659–2673. doi: 10.1038/s41380-022-01511-z
4. Sweeney MD, Zhao Z, Montagne A, Nelson AR, Zlokovic BV. From physiology to disease and Back. *Physiol Rev*. 2019;99:21–78. doi: 10.1152/physrev.00050.2017
5. Zlokovic BV. The blood-brain barrier in health and chronic neurodegenerative disorders. *Neuron*. 2008;57:178–201. doi: 10.1016/j.neuron.2008.01.003
6. Sweeney MD, Kisler K, Montagne A, Toga AW, Zlokovic BV. The role of brain vasculature in neurodegenerative disorders. *Nat Neurosci*. 2018;21:1318–1331. doi: 10.1038/s41593-018-0234-x
7. Armulik A, Genové G, Mäe M, Nisancioglu MH, Wallgard E, Niaudet C, He L, Norlin J, Lindblom P, Strittmatter K, et al. Pericytes regulate the blood-brain barrier. *Nature*. 2010;468:557–561. doi: 10.1038/nature09522
8. Daneman R, Zhou L, Kebede AA, Barres BA. Pericytes are required for blood-brain barrier integrity during embryogenesis. *Nature*. 2010;468:562–566. doi: 10.1038/nature09513
9. Longden TA, Zhao G, Hariharan A, Lederer WJ. Pericytes and the control of blood flow in brain and heart. *Annu Rev Physiol*. 2023;85:137–164. doi: 10.1146/annurev-physiol-031522-034807
10. Hariharan A, Robertson CD, Garcia DCG, Longden TA. Brain capillary pericytes are metabolic sentinels that control blood flow through a KATP channel-dependent energy switch. *Cell Rep*. 2022;41:111872. doi: 10.1016/j.celrep.2022.111872
11. Eilken HM, Diéguez-Hurtado R, Schmidt I, Nakayama M, Jeong HW, Arf H, Adams S, Ferrara N, Adams RH. Pericytes regulate VEGF-induced endothelial sprouting through VEGFR1. *Nat Commun*. 2017;8:8. doi: 10.1038/s41467-017-01738-3
12. Török O, Schreiner B, Schaffenrath J, Tsai H-C, Maheshwari U, Stifter SA, Welsh C, Amorim A, Sridhar S, Utz SG, et al. Pericytes regulate vascular immune homeostasis in the CNS. *Proc Natl Acad Sci U S A*. 2021;118(10):e2016587118. doi: 10.1073/pnas.2016587118
13. Stark K, Eckart A, Haidari S, Tirniceriu A, Lorenz M, Von Brühl ML, Gärtner F, Khandoga AG, Legate KR, Pless R, et al. Capillary and arteriolar pericytes attract innate leukocytes exiting through venules and "instruct" them with pattern-recognition and motility programs. *Nat Immunol*. 2013;14:41–51. doi: 10.1038/ni.2477
14. Proebstl D, Voisin MB, Woodfin A, Whiteford J, D'Acquisto F, Jones GE, Rowe D, Nourshargh S. Pericytes support neutrophil subendothelial cell crawling and breaching of venular walls in vivo. *J Exp Med*. 2012;209:1219–1234. doi: 10.1084/jem.20111622
15. Rustenhoven J, Jansson D, Smyth LC, Dragunow M. Brain Pericytes As mediators of Neuroinflammation. *Trends Pharmacol Sci*. 2017;38:291–304. doi: 10.1016/j.tips.2016.12.001
16. Dalkara T, Gursoy-Ozdemir Y, Yemisci M. Brain microvascular pericytes in health and disease. *Acta Neuropathol*. 2011;122:1–9. doi: 10.1007/s00401-011-0847-6
17. Uemura MT, Maki T, Ihara M, Lee VMY, Trojanowski JQ. Brain microvascular Pericytes in vascular cognitive impairment and dementia. *Front Aging Neurosci*. 2020;12:12. doi: 10.3389/fnagi.2020.00080
18. Berthiaume AA, Schmid F, Stamenkovic S, Coelho-Santos V, Nielson CD, Weber B, Majesky MW, Shih AY. Pericyte remodeling is deficient in the aged brain and contributes to impaired capillary flow and structure. *Nat Commun*. 2022;13:13. doi: 10.1038/s41467-022-33464-w
19. Kofler NM, Cuervo H, Uh MK, Murtomäki A, Kitajewski J. Combined deficiency of Notch1 and Notch3 causes pericyte dysfunction, models CADASIL, and results in arteriovenous malformations. *Sci Rep*. 2015;5:5. doi: 10.1038/srep16449
20. Kisler K, Nelson AR, Rege SV, Ramanathan A, Wang Y, Ahuja A, Lazic D, Tsai PS, Zhao Z, Zhou Y, et al. Pericyte degeneration leads to neurovascular uncoupling and limits oxygen supply to brain. *Nat Neurosci*. 2017;20:406–416. doi: 10.1038/nn.4489
21. Sweeney MD, Ayyadurai S, Zlokovic BV. Pericytes of the neurovascular unit: key functions and signaling pathways. *Nat Neurosci*. 2016;19:771–783. doi: 10.1038/nn.4288
22. Ungvari Z, Toth P, Tarantini S, Prodan CI, Sorond F, Merkely B, Csiszar A. Hypertension-induced cognitive impairment: from pathophysiology to public health. *Nat Rev Nephrol*. 2021;17:639–654. doi: 10.1038/s41581-021-00430-6
23. Fang C, Magaki SD, Kim RC, Kalaria RN, Vinters HV, Fisher M. Arteriolar neuropathology in cerebral microvascular disease. *Neuropathol Appl Neurobiol*. 2023;49:e12875. doi: 10.1111/nan.12875
24. Schreiber S, Bueche CZ, Garz C, Braun H. Blood brain barrier breakdown as the starting point of cerebral small vessel disease?—New insights from a rat model. *Exp Transl Stroke Med*. 2013;5:5. doi: 10.1186/2040-7378-5-4
25. Evans LE, Taylor JL, Smith CJ, Pritchard HAT, Greenstein AS, Allan SM. Cardiovascular comorbidities, inflammation, and cerebral small vessel disease. *Cardiovasc Res*. 2021;117:2575–2588. doi: 10.1093/cvr/cvab284
26. Pantoni L. Cerebral small vessel disease: from pathogenesis and clinical characteristics to therapeutic challenges. *Lancet Neurol*. 2010;9:689–701. doi: 10.1016/S1474-4422(10)70104-6
27. Wardlaw JM, Smith C, Dichgans M. Small vessel disease: mechanisms and clinical implications. *Lancet Neurol*. 2019;18:684–696. doi: 10.1016/S1474-4422(19)30079-1
28. Quick S, Moss J, Rajani RM, Williams A. A vessel for change: endothelial dysfunction in cerebral small vessel disease. *Trends Neurosci*. 2021;44:289–305. doi: 10.1016/j.tins.2020.11.003
29. Morton L, Arndt P, Garza AP, Henneicke S, Mattern H, Gonzalez M, Dityatev A, Yilmazer-Hanke D, Schreiber S, Dunay IR. Spatio-temporal dynamics of microglia phenotype in human and murine cSVD: impact of acute and chronic hypertensive states. *Acta Neuropathol Commun*. 2023;11:11. doi: 10.1186/s40478-023-01672-0
30. Blevins BL, Vinters HV, Love S, Wilcock DM, Grinberg LT, Schneider JA, Kalaria RN, Katsumata Y, Gold BT, Wang DJJ, et al. Brain arteriolosclerosis. *Acta Neuropathol*. 2021;141:1–24. doi: 10.1007/s00401-020-02235-6
31. Buzas EI. The roles of extracellular vesicles in the immune system. *Nat Rev Immunol*. 2022;23:236–250. doi: 10.1038/s41577-022-00763-8
32. Crewe C, Funcke JB, Li S, Joffin N, Gliniak CM, Ghaben AL, An YA, Sadek HA, Gordillo R, Akgul Y, et al. Extracellular vesicle-based interorgan transport of mitochondria from energetically stressed adipocytes. *Cell Metab*. 2021;33:1853–1868.e11. doi: 10.1016/j.cmet.2021.08.002
33. Van Niel G, D'Angelo G, Raposo G. Shedding light on the cell biology of extracellular vesicles. *Nat Rev Mol Cell Biol*. 2018;19:213–228. doi: 10.1038/nrm.2017.125
34. Bailey EL, Mcbride MW, Beattie W, Mcclure JD, Graham D, Dominiczak AF, Sudlow CLM, Smith C, Wardlaw JM. Differential gene expression in multiple neurological, inflammatory and connective tissue pathways in a spontaneous model of human small vessel stroke. *Neuropathol Appl Neurobiol*. 2014;40:855–872. doi: 10.1111/nan.12116
35. Bailey EL, Wardlaw JM, Graham D, Dominiczak AF, Sudlow CLM, Smith C. Cerebral small vessel endothelial structural changes predate hypertension in stroke-prone spontaneously hypertensive rats: a blinded, controlled immunohistochemical study of 5- to 21-week-old rats. *Neuropathol Appl Neurobiol*. 2011;37:711–726. doi: 10.1111/j.1365-2990.2011.01170.x

36. Held F, Morris AWJ, Pirici D, Niklass S, Sharp MMG, Garz C, Assmann A, Heinze HJ, et al. Vascular basement membrane alterations and β-amyloid accumulations in an animal model of cerebral small vessel disease. *Clin Sci*. 2017;131:1001–1013. doi: 10.1042/CS20170004
37. Jandke S, Garz C, Schwanke D, Sendtner M, Heinze HJ, Carare RO, Schreiber S. The association between hypertensive arteriopathy and cerebral amyloid angiopathy in spontaneously hypertensive stroke-prone rats. *Brain Pathol*. 2018;28:844–859. doi: 10.1111/bpa.12629
38. Kaiser D, Weise G, Möller K, Scheibe J, Pösel C, Baasch S, Gawlitza M, Lobsien D, Diederich K, Minnerup J, et al. Spontaneous white matter damage, cognitive decline and neuroinflammation in middle-aged hypertensive rats: An animal model of early-stage cerebral small vessel disease. *Acta Neuropathol Commun*. 2014;2:169. doi: 10.1186/s40478-014-0169-8
39. He L, Vanlandewijck M, Raschperger E, Andaloussi Maë M, Jung B, Lebouvier T, Ando K, Hofmann J, Keller A, Betsholtz C. Analysis of the brain mural cell transcriptome. *Sci Rep*. 2016;6:6. doi: 10.1038/srep35108
40. Vanlandewijck M, He L, Mäe MA, Andrae J, Ando K, Del Gaudio F, Nahar K, Lebouvier T, Laviña B, Gouveia L, et al. A molecular atlas of cell types and zonation in the brain vasculature. *Nature*. 2018;554:475–480. doi: 10.1038/nature25739
41. Percie du Sert N, Hurst V, Ahluwalia A, Alam S, Avey MT, Baker M, Browne WJ, Clark A, Cuthill IC, Dirnagl U, et al. The ARRIVE Guidelines 2.0: updated guidelines for reporting animal research. *PLoS Biol*. 2020;18(7):e3000410. doi: 10.1371/journal.pbio.3000410
42. Schreiber S, Bueche CZ, Garz C, Kropf S, Angenstein F, Goldschmidt J, Neumann J, Heinze HJ, Goertler M, Reymann KG, et al. The pathologic cascade of cerebrovascular lesions in SHRSP: is erythrocyte accumulation an early phase. *J Cereb Blood Flow Metab*. 2012;32:278–290. doi: 10.1038/jcbfm.2011.122
43. Crouch EE, Doetsch F. FACS isolation of endothelial cells and pericytes from mouse brain microregions. *Nat Protoc*. 2018;13:738–751. doi: 10.1038/nprot.2017.158
44. Nakagawa S, Deli MA, Kawaguchi H, Shimizudani T, Shimono T, Kittel Á, Tanaka K, Niwa M. A new blood-brain barrier model using primary rat brain endothelial cells, pericytes and astrocytes. *Neurochem Int*. 2009;54:253–263. doi: 10.1016/j.neuint.2008.12.002
45. Lee YK, Uchida H, Smith H, Ito A, Sanchez T. The isolation and molecular characterization of cerebral microvessels. *Nat Protoc*. 2019;14:3059–3081. doi: 10.1038/s41596-019-0212-0
46. Livak KJ, Schmittgen TD. Analysis of relative gene expression data using real-time quantitative PCR and the 2-ΔΔCT method. *Methods*. 2001;25:402–408. doi: 10.1006/meth.2001.1262
47. Shihan MH, Novo SG, Le Marchand SJ, Wang Y, Duncan MK. A simple method for quantitating confocal fluorescent images. *Biochem Biophys Rep*. 2021;25:25. doi: 10.1016/j.bbrep.2021.100916
48. Garza AP, Morton L, Pállinger É, Buzás EI, Schreiber S, Schott BH, Dunay IR. Initial and ongoing tobacco smoking elicits vascular damage and distinct inflammatory response linked to neurodegeneration. *Brain Behav Immun Health*. 2023;28:100597. doi: 10.1016/j.bbih.2023.100597
49. Debska-Vielhaber G, Miller I, Peeva V, Zuschratter W, Walczak J, Schreiber S, Petri S, Machts J, Vogt S, Szczepanowska J, et al. Impairment of mitochondrial oxidative phosphorylation in skin fibroblasts of SALS and FALS patients is rescued by in vitro treatment with ROS scavengers. *Exp Neurol*. 2021;339:113620. doi: 10.1016/j.expneurol.2021.113620
50. Kirkman DL, Robinson AT, Rossman MJ, Seals DR, Edwards DG. Mitochondrial contributions to vascular endothelial dysfunction, arterial stiffness, and cardiovascular diseases. *Am J Physiol Heart Circ Physiol*. 2021;320:H2080–H2100. doi: 10.1152/ajpheart.00917.2020
51. Biswas SK. Metabolic reprogramming of immune cells in cancer progression. *Immunity*. 2015;43:435–449. doi: 10.1016/j.immuni.2015.09.001
52. Pålsson-McDermott EM, O'Neill LAJ. Targeting immunometabolism as an anti-inflammatory strategy. *Cell Res*. 2020;30:300–314. doi: 10.1038/s41422-020-0291-z
53. Pereira FE, Cronin C, Ghosh M, Zhou SY, Agosto M, Subramani J, Wang R, Shen JB, Schacke W, Liang B, et al. CD13 is essential for inflammatory trafficking and infarct healing following permanent coronary artery occlusioninmice. *Cardiovasc Res*. 2013;100:74–83. doi: 10.1093/cvr/cvt155
54. Ghosh M, Gerber C, Rahman MM, Vernier KM, Pereira FE, Subramani J, Caromile LA, Shapiro LH. Molecular mechanisms regulating CD13-mediated adhesion. *Immunology*. 2014;142:636–647. doi: 10.1111/imm.12279
55. Ito M, Oliveriot MI, Mannont PJ, Bestt CF, Maeda N, Smithies O, Coffmanu TM. Regulation of blood pressure by the type 1A angiotensin II receptor gene (gene targeting/G protein-coupled receptor/hypertension). *Proc Natl Acad Sci U S A*. 1995;92:3521–3525. doi: 10.1073/pnas.92.8.3521
56. Nataraj C, Oliverio MI, Mannon RB, Mannon PJ, Audoly LP, Amuchastegui CS, Ruiz P, Smithies O, Coffman TM. Angiotensin II regulates cellular immune responses through a calcineurin-dependent pathway. *J Clin Investig*. 1999;104:1693–1701. doi: 10.1172/JCI7451
57. Benigni A, Corna D, Zoja C, Sonzogni A, Latini R, Salio M, Conti S, Rottoli D, Longaretti L, Cassis P, et al. Disruption of the Ang II type 1 receptor promotes longevity in mice. *J Clin Investig*. 2009;119:524–530. doi: 10.1172/JCI36703
58. Paillard F, Chansel D, Brand E, Benetos A, Thomas F, Czekalski S, Ardaillou R, Soubrier F. Genotype-phenotype relationships for the renin-angiotensin-aldosterone system in a Normal population. 1999;34:423–429. doi: 10.1161/01.HYP.34.3.423
59. Cober ND, Mccourt E, Soares Godoy R, Deng Y, Schlosser K, Situ A, Cook DP, Lemay S-E, Klouda T, Yuan K, et al. Emergence of disease specific endothelial and stromal cell populations involved in arterial remodeling during development of pulmonary arterial hypertension. doi: 10.1101/2023.09.06.555321
60. Wang YY, Pan LY, Moens CB, Appel B. Notch3 establishes brain vascular integrity by regulating pericyte number. *Development (Cambridge)*. 2014;141:307–317. doi: 10.1242/dev.096107
61. Tefft JB, Bays JL, Lammers A, Kim S, Eyckmans J, Chen CS. Notch1 and Notch3 coordinate for pericyte-induced stabilization of vasculature. *Am J Physiol Cell Physiol*. 2022;322:C185–C196. doi: 10.1152/ajpcell.00320.2021
62. Rana R, Huang T, Koukos G, Fletcher EK, Turner SE, Shearer A, Gurbel PA, Rade JJ, Kimmelstiel CD, Bliden KP, et al. Noncanonical matrix metalloprotease 1-protease activated receptor 1 signaling drives progression of atherosclerosis. *Arterioscler Thromb Vasc Biol*. 2018;38:1368–1380. doi: 10.1161/ATVBAHA.118.310967
63. Boyalla V, Gallego-Colon E, Spartalis M. Immunity and inflammation in cardiovascular disorders. *BMC Cardiovasc Disord*. 2023;23:148. doi: 10.1186/s12872-023-03185-z
64. Piaszyk-Borychowska A, Széles L, Csermely A, Chiang HC, Wesoły J, Lee CK, Nagy L, Bluyssen HAR. Signal integration of IFN-I and IFN-II with TLR4 involves sequential recruitment of STAT1-complexes and NFκB to enhance pro-inflammatory transcription. *Front Immunol*. 2019;10:10. doi: 10.3389/fimmu.2019.01253
65. Brasier AR. The nuclear factor-B-interleukin-6 signalling pathway mediating vascular inflammation. *Cardiovasc Res*. 2010;86:211–218. doi: 10.1093/cvr/cvq076
66. Warner SJC, Auger KR, Libby P. Human interleukin 1 induces interleukin 1 gene expression in human vascular smooth muscle cells. *J Exp Med*. 1987;165(5):1316–1331. doi: 10.1084/jem.165.5.1316
67. Khyzha N, Khor M, Distefano PV, Wang L, Matic L, Hedin U, Wilson MD, Maegdefessel L, Fish JE. Regulation of CCL2 expression in human vascular endothelial cells by a neighboring divergently transcribed long noncoding RNA. *PNAS*. 2019:16410–16419. doi: 10.1073/pnas.1904108116
68. Elhage R, Ljunggren HG, Hansson GK. Proatherogenic role of interleukin-18: effects on inflammation and action on vascular cells. *Cardiovasc Res*. 2012;96:176–180. doi: 10.1093/cvr/cvs220
69. Kim HY, Kim HS. IL-10 up-regulates CCL5 expression in vascular smooth muscle cells from spontaneously hypertensive rats. *Cytokine*. 2014;68:40–49. doi: 10.1016/j.cyto.2014.02.008
70. Ebrahem Q, Chaurasia SS, Vasanji A, Qi JH, Klenotic PA, Cutler A, Asosingh K, Erzurum S, Anand-Apte B. Cross-talk between vascular endothelial growth factor and matrix metalloproteinases in the induction of neovascularization in vivo. *Am J Pathol*. 2010;176:496–503. doi: 10.2353/ajpath.2010.080642
71. Lee S, Jilan SM, Nikolova GV, Carpizo D, Luisa Iruela-Arispe M. Processing of VEGF-A by matrix metalloproteinases regulates bioavailability and vascular patterning in tumors. *J Cell Biol*. 2005;169:681–691. doi: 10.1083/jcb.200409115

72. Ahmad A, Nawaz MI. Molecular mechanism of VEGF and its role in pathological angiogenesis. *J Cell Biochem*. 2022;123:1938–1965. doi: 10.1002/jcb.30344
73. Tsang CK w, Liu Y, Thomas J, Zhang Y, Zheng XFS. Superoxide dismutase 1 acts as a nuclear transcription factor to regulate oxidative stress resistance. *Nat Commun*. 2014;5:3446. doi: 10.1038/ncomms4446
74. Griendling KK, Camargo LL, Rios FJ, Alves-Lopes R, Montezano AC, Touyz RM. Oxidative stress and hypertension. *Circ Res*. 2021;128:993–1020. doi: 10.1161/CIRCRESAHA.121.318063
75. Ward PS, Thompson CB. Metabolic reprogramming: a cancer Hallmark even Warburg did not anticipate. *Cancer Cell*. 2012;21:297–308. doi: 10.1016/j.ccr.2012.02.014
76. Wang Y, Patti GJ. The Warburg effect: a signature of mitochondrial overload. *Trends Cell Biol*. 2023;33:1014–1020. doi: 10.1016/j.tcb.2023.03.013
77. Brier MR, Blazey T, Raichle ME, Morris JC, Benzinger TLS, Vlassenko AG, Snyder AZ, Goyal MS. Increased white matter glycolysis in humans with cerebral small vessel disease. *Nat Aging*. 2022;2:991–999. doi: 10.1038/s43587-022-00303-y